tion of Biopharmaceuticals. American Association of Pharmaceutical Scientsits, Arlington, pp. 139–228.
Costantino, H.R., Carrasquillo, K.G., Cordero, R.A., Mumenthaler, M., Hsu, C.C., Griebenow, K., 1998. Effect of excipients on the stability and structure of lyophilized recombinant human growth hormone. J. Pharm. Sci. 87, 1412–1420.
Desai, D., Rao, V., Guo, H., Li, D., Bolgar, M., 2007. Stability of low concentrations of guanine-based antivirals in sucrose or maltitol solutions. Int. J. Pharm. 342, 87–94.
Dong, A., Prestrelski, S.J., Allison, S.D., Carpenter, J.F., 1995. Infrared spectroscopic studies of lyophilization- and temperature-induced protein aggregation. J. Pharm. Sci. 84, 415–424.
Franks, F., 1992. Freeze-drying: from empiricism to predictability. The significance of glass transitions. Dev. Biol. Stand. 74, 9–18.
Gekko, K., 1982. Calorimetric study on thermal denaturation of lysozyme in polyol-water mixtures. J. Biochem. 91, 1197–1204.
Gekko, K., Idota, Y., 1989. Amino acid solubility and protein stability in aqueous maltitol solutions. Agric. Biol. Chem. 53, 89–95.
Griebenow, K., Klibanov, A.M., 1995. Lyophilization-induced reversible changes in the secondary structure of proteins. Proc. Natl. Acad. Sci. U.S.A. 92, 10969–10976.
Hancock, B.C., Shamblin, S.L., Zografi, G., 1995. Molecular mobility of amorphous pharmaceutical solids below their glass transition temperatures. Pharm. Res. 12, 799–806.
Hermeling, S., Crommelin, D.J., Schellekens, H., Jiskoot, W., 2004. Structure-immunogenicity relationships of therapeutic proteins. Pharm. Res. 21, 897–903.
Izutsu, K., Aoyagi, N., Kojima, S., 2004. Protection of protein secondary structure by saccharides of different molecular weights during freeze-drying. Chem. Pharm. Bull. 52, 199–203.
Izutsu, K., Kadoya, S., Yomota, C., Kawanishi, T., Yonemochi, E., Terada, K., 2009. Freeze-drying of proteins in glass solids formed by basic amino acids and dicarboxylic acids. Chem. Pharm. Bull. 57, 43–48.
Izutsu, K., Yoshioka, S., Terao, T., 1993. Decreased protein-stabilizing effects of cryoprotectants due to crystallization. Pharm. Res. 10, 1232–1237.
Izutsu, K., Yoshioka, S., Terao, T., 1994. Stabilizing effect of amphiphilic excipients on the freeze-thawing and freeze-drying of lactate dehydrogenase. Biotechnol. Bioeng. 43, 1102–1107.
Jaenicke, R., 1990. Protein structure and function at low-temperatures. Philos. Trans. R. Soc. Lond. B Biol. Sci. 326, 535–551.
Jiang, S., Nail, S.L., 1998. Effect of process conditions on recovery of protein activity after freezing and freeze-drying. Eur. J. Pharm. Biopharm. 45, 249–257.
Johnson, R.E., Kirchhoff, C.F., Gaud, H.T., 2002. Mannitol-sucrose mixtures–versatile formulations for protein lyophilization. J. Pharm. Sci. 91, 914–922.
Kawai, K., Hagiwara, T., Takai, R., Suzuki, T., 2004. Maillard reaction rate in various glassy matrices. Biosci. Biotechnol. Biochem. 68, 2285–2288.
Levine, H., Slade, L., 1988. Thermomechanical properties of small-carbohydrate-water glasses and rubbers. Kinetically metastable systems at sub-zero temperatures. J. Chem. Soc., Faraday Trans. 1 84, 2619–2633.
Liao, Y.H., Brown, M.B., Quader, A., Martin, G.P., 2002. Protective mechanism of stabilizing excipients against dehydration in the freeze-drying of proteins. Pharm. Res. 19, 1854–1861.
Manning, M.C., Patel, K., Borchardt, R.T., 1989. Stability of protein pharmaceuticals. Pharm. Res. 6, 903–918.
Meister, E., Gieseler, H., 2009. Freeze-dry microscopy of protein/sugar mixtures: Drying behavior, interpretation of collapse temperatures and a comparison to corresponding glass transition data. J. Pharm. Sci. 98, 3072–3087.
Miller, D.P., Anderson, R.E., de Pablo, J.J., 1998. Stabilization of lactate dehydrogenase following freeze-thawing and vacuum-drying in the presence of trehalose and borate. Pharm Res. 15, 1215–1221.
Nail, S.L., Jiang, S., Chongprasert, S., Knopp, S.A., 2002. Fundamentals of freeze-drying. Pharm. Biotechnol. 14, 281–360.
Ohtake, S., Schebor, C., Palecek, S.P., de Pablo, J.J., 2004. Effect of pH, counter ion, and phosphate concentration on the glass transition temperature of freeze-dried sugar-phosphate mixtures. Pharm. Res. 21, 1615–1621.
Perez Locas, C., Yaylayan, V.A., 2008. Isotope labeling studies on the formation of 5-(hydroxymethyl)-2-furaldehyde (HMF) from sucrose by pyrolysis-GC/MS. J. Agric. Food Chem. 56, 6717–6723.
Piedmonte, D.M., Summers, C., McAuley, A., Karamujic, L., Ratnaswamy, G., 2007. Sorbitol crystallization can lead to protein aggregation in frozen protein formulations. Pharm. Res. 24, 136–146.
Pikal, M.J., Shah, S., 1990. The collapse temperature in freeze-drying: dependence on measurement methodology and rate of water removal from the glassy phase. Int. J. Pharm. 62, 165–186.
Prestrelski, S.J., Tedeschi, N., Arakawa, T., Carpenter, J.F., 1993. Dehydration-induced conformational transitions in proteins and their inhibition by stabilizers. Biophys. J. 65, 661–671.
Shirke, S., Takhistov, P., Ludescher, R.D., 2005. Molecular mobility in amorphous maltose and maltitol from phosphorescence of erythrosin B. J. Phys. Chem. B 109, 16119–16126.
Slade, L., Levine, H., Ievolella, J., Wang, M., 2006. The glassy state phenomenon in applications for the food industry: application of the food polymer science approach to structure-function relationships of sucrose in cookie and cracker systems. J. Sci. Food Agric. 63, 133–176.
Suzuki, T., 1981. Fish and Krill Protein: Processing Technology. Applied Science Publishers, London.
Tamoto, K., Tanaka, S., Takeda, F., Fukumi, T., Nishiya, K., 1961. Studies on freezing of surimi and its application. IV. On the effect of sugar upon the keeping quality of frozen Alsaka pollock meat. Bull. Hokkaido Reg. Fish Res. Lab. 23, 50–60.
Tanaka, K., Takeda, T., Miyajima, K., 1991. Cryoprotection effect of saccharides on denaturation of catalase by freeze-drying. Chem. Pharm. Bull. 39, 1091–1094.
Tian, F., Middaugh, C.R., Offerdahl, T., Munson, E., Sane, S., Rytting, J.H., 2007. Spectroscopic evaluation of the stabilization of humanized monoclonal antibodies in amino acid formulations. Int. J. Pharm. 335, 20–31.
Wang, W., 2000. Lyophilization and development of solid protein pharmaceuticals. Int. J. Pharm. 203, 1–60.

Importance of Neonatal FcR in Regulating the Serum Half-Life of Therapeutic Proteins Containing the Fc Domain of Human IgG1: A Comparative Study of the Affinity of Monoclonal Antibodies and Fc-Fusion Proteins to Human Neonatal FcR

Takuo Suzuki,* Akiko Ishii-Watabe,* Minoru Tada,* Tetsu Kobayashi,* Toshie Kanayasu-Toyoda,* Toru Kawanishi,† and Teruhide Yamaguchi*

The neonatal FcR (FcRn) binds to the Fc domain of IgG at acidic pH in the endosome and protects IgG from degradation, thereby contributing to the long serum half-life of IgG. To date, more than 20 mAb products and 5 Fc-fusion protein products have received marketing authorization approval in the United States, the European Union, or Japan. Many of these therapeutic proteins have the Fc domain of human IgG1; however, the serum half-lives differ in each protein. To elucidate the role of FcRn in the pharmacokinetics of Fc domain-containing therapeutic proteins, we evaluated the affinity of the clinically used human, humanized, chimeric, or mouse mAbs and Fc-fusion proteins to recombinant human FcRn by surface plasmon resonance analysis. The affinities of these therapeutic proteins to FcRn were found to be closely correlated with the serum half-lives reported from clinical studies, suggesting the important role of FcRn in regulating their serum half-lives. The relatively short serum half-life of Fc-fusion proteins was thought to arise from the low affinity to FcRn. The existence of some mAbs having high affinity to FcRn and a short serum half-life, however, suggested the involvement of other critical factor(s) in determining the serum half-life of such Abs. We further investigated the reason for the relatively low affinity of Fc-fusion proteins to FcRn and suggested the possibility that the receptor domain of Fc-fusion protein influences the structural environment of the FcRn binding region but not of the FcγRI binding region of the Fc domain. ***The Journal of Immunology*****, 2010, 184: 1968–1976.**

In healthy humans, IgG1 exhibits a long serum half-life of ~21 d (1). This prolonged half-life of IgG can be explained by the interaction with neonatal FcR (FcRn). FcRn is a heterodimer of the MHC class I-like H chain and the β_2-microglobulin (β_2m) L chain (2). Although this receptor was originally studied as a transporter of IgG from mother to fetus, subsequent studies have shown that this receptor also plays a critical role in regulating IgG homeostasis (3, 4). FcRn binds to the Fc domain of IgG at pH 6.0–6.5 but not, or weakly, at pH 7.0–7.5 (5). Therefore, FcRn protects IgG from degradation by binding to IgG in endosome and releases IgG into plasma (6). As indicated by previous studies in which amino acid substitutions in the Fc domain of IgG for modifying the affinity to FcRn can alter the serum half-life of the IgG, the affinity to FcRn is thought to play a critical role in determining the serum half-life of IgG (7–12).

Recently, therapeutic use of mAb products has become more important for various diseases, including cancer as well as autoimmune and infectious diseases (6, 13, 14). In addition to the mAbs, the Fc-fusion proteins (e.g., etanercept, alefacept, and abatacept) have been developed and have received considerable attention. These Fc-fusion proteins consist of an extracellular domain of membrane receptor linked to the Fc portion of human IgG1. They work like Abs by binding to ligands for the receptors. The receptor portions of etanercept and alefacept are, respectively, the extracellular ligand-binding portion of the human 75-kDa TNFR and the extracellular CD2-binding portion of the human leukocyte function Ag 3. Abatacept consists of the extracellular domain of human CTLA-4 linked to the modified Fc portion of human IgG1.

Most of the mAb products and Fc-fusion protein products have the Fc domain of human IgG1 (6, 14). Accumulating evidence regarding their clinical use has revealed that their serum half-lives are variable, ranging from 4 to 23 d, regardless of the presence of the Fc domain of human IgG1 (6). Although many factors such as m.w., posttranslational modifications including glycosylation, electrical properties, interactions with FcRs or target molecules, and features of the target molecules may influence their serum half-life, the reasons for the variability of half-life have not been elucidated. Among such factors, FcRn might play a critical role in regulating half-life; however, comparative studies between the affinities of these therapeutic proteins to FcRn and their half-lives in humans have not been reported. Therefore, although some Fc domain-containing therapeutic proteins exhibit shorter half-lives in humans, it remains unclear whether the shorter half-lives are due to the lower affinity to FcRn or other factors.

*Division of Biological Chemistry and Biologicals and †Division of Drugs, National Institute of Health Sciences, Tokyo, Japan

Received for publication October 8, 2009. Accepted for publication December 16, 2009.

This work was supported in part by Grant-in-Aid for Young Scientists 21790172 from the Ministry of Education, Culture, Sports, Science, and Technology, and Grants-in-Aid for Scientific Research 18590163 and 20590167 from Japan Society for the Promotion of Science.

Address correspondence and reprint requests to Dr. Akiko Ishii-Watabe, National Institute of Health Sciences, 1-18-1 Kamiyoga, Setagaya-ku, Tokyo 158-8501, Japan. E-mail address: watabe@nihs.go.jp

Abbreviations used in this paper: β_2m, β_2-microglobulin; FcRn, neonatal FcR; HER2, human epidermal growth factor receptor 2; ND, not detected; R^2, coefficient of determination; SPR, surface plasmon resonance.

www.jimmunol.org/cgi/doi/10.4049/jimmunol.0903296

In this study, we examined the affinity of clinically used mAbs and Fc-fusion proteins to recombinant human FcRn by surface plasmon resonance (SPR) analysis. The analytes used were human Ab (adalimumab), humanized Abs (daclizumab, omalizumab, palivizumab, and trastuzumab), chimeric Abs (infliximab and rituximab), mouse Ab (muromonab-CD3), and Fc-fusion proteins (etanercept, alefacept, and abatacept). We found that the affinities of the therapeutic proteins tested to FcRn were closely correlated with their serum half-lives, with a few exceptions. Because Fc-fusion proteins, which have relatively short half-lives (4–13 d), were shown to have lower affinity to FcRn than mAbs, we further investigated the reason for this difference by examining the affinity of the proteins to FcγRI or the affinity of papain-digested proteins to FcRn in SPR analyses. Our results suggested the possibility that the receptor portions of Fc-fusion proteins make a difference in the higher-order structure of the FcRn-binding region of Fc (i.e., CH2-CH3 interface) or interfere with binding between the Fc domain and FcRn by steric hindrance.

Materials and Methods

Therapeutic proteins and reagents

Abatacept (Bristol-Myers Squibb, Princeton, NJ), adalimumab (Abbott, Baar, Switzerland), alefacept (Biogen Idec, Cambridge, MA), daclizumab (Hoffmann-La Roshe, Nutley, NJ), etanercept (Takeda Pharmaceutical, Osaka, Japan), infliximab (Tanabe Phamaceutical, Osaka, Japan), muromonab-CD-3 (Jansen Pharmaceutical, Tokyo, Japan), omalizumab (Novartis Pharma Schweiz, Bern, Switzerland), palivizumab (Abbott Japan, Osaka, Japan), rituximab (Zenyaku Kogyo, Tokyo, Japan), and trastuzumab (Chugai Pharmaceutical, Tokyo, Japan) were purchased via reagent distributors. Recombinant human TNF-α was purchased from Wako (Osaka, Japan).

Purification of human FcRn

Stably transfected CHO cells expressing both the soluble portion of the hFcRn H chain (residues 1–267 of mature protein) and β_2m were provided by P. J. Bjorkman (California Institute of Technology, Pasadena, CA). Expression and purification of hFcRn were performed according to the method previously reported by West and Bjorkman (15), with slight modifications. Briefly, the CHO cells expressing soluble hFcRn and β_2m were cultured in α-MEM containing 5% dialyzed FBS, 100 μM methionine sulfoximine, and penicillin/streptomycin. Cell culture supernatant was collected every 2–3 d and was filtered with a 0.45-μm filter, and sodium azide was then added to 0.05%. The harvested supernatant was acidified to pH 5.8 and then applied to a human IgG column. After washing the column with 50 mM Bis-Tris (pH 5.8), hFcRn complexed with β_2m was eluted with 40 mM Bis-Tris/20 mM Tris (pH 8.1). The eluted fractions containing hFcRn were applied to a Uno-Q1 column, and hFcRn was eluted with pH gradient using 40 mM Bis-Tris/20 mM Tris (pH 8.1) and 40 mM Bis-Tris/20 mM Tris (pH 5.8).

SDS-PAGE and Western blotting

Each fraction of protein eluted from the Uno-Q1column was diluted in 1× SDS loading buffer and was separated in 15% polyacrylamide gel (Bio craft, Tokyo, Japan). After the electrophoresis, the gels were stained with Imperial protein stain (Pierce, Rockford, IL). For Western blotting, proteins separated by SDS-PAGE were electroblotted onto polyvinylidene difluoride membranes (Millipore, Billerica, MA). The membranes were immunoreacted with rabbit anti-hFcRn H chain peptide (Leu^{135}-Gly^{148}) Ab produced by Medical and Biological Laboratories (Nagoya, Japan) and then with HRP-conjugated secondary Abs (Cell Signaling Technology, Danvers, MA). The bands of hFcRn were detected using ECL Plus Western blotting detection reagents (Amersham Biosciences, Piscataway, NJ).

SPR analyses

Analysis of affinity between FcRn and Fc domain-containing therapeutic proteins. The purified recombinant hFcRn was diluted with 10 mM sodium acetate (pH 5.0 or 4.5) and was immobilized onto a CM5 biosensor chip (Biacore, Uppsala, Sweden) using an amine coupling kit (Biacore) at relatively low densities (mainly 300–350 resonance units) to avoid mass transport limitation. The reference cell was treated with *N*-hydroxysuccinimide/1-ethyl-3-(3-dimethylaminopropyl) carbodiimide and ethanol amine using an amine coupling kit without injecting the FcRn. Fc domain-containing proteins were diluted with the running buffer (50 mM sodium phosphate/150 mM NaCl [pH 6.0]) and injected at 25°C. The running buffer was allowed to flow at a rate of 20 μl/min. The injections were performed using the KINJECT mode (volume, 40 μl; dissociation time, 150 s). For regeneration, the regeneration buffer (100 mM Tris/200 mM NaCl [pH 8.0]) was injected for 4 min. Kinetic constants were calculated from the sensorgrams using the bivalent analyte model of BIAevaluation software 4.1.

To obtain the consistent results, we would indicate two points. First, it is necessary to set the bulk refractive index to zero to avoid wrong fitting, because the binding is rapidly reached to the near-equilibrium state. Second, it is necessary to set the injection point correctly. For example, if the sensorgrams of infliximab shown in Fig. 2 were analyzed with the injection point shifted to 0.5 s earlier, the values of k_{a1}, k_{d1}, and K_D were 1.95E+05 $M^{-1}s^{-1}$, 0.136 s^{-1}, and 697 nM, respectively. When the injection points of the sensorgrams are unclear, it may be better to use the average values of data resulting from two or more different injection points.

Analysis of affinity between FcγRI and Fc domain-containing therapeutic proteins. Recombinant human FcγRI, which consists of human FcγRI (Gln^{16}-Pro^{288}) and His-tag, was purchased from R&D Systems (Minneapolis, MN). Fc domain-containing proteins were immobilized to a CM5 biosensor chip in 10 mM sodium acetate (pH 5.0) using an amine coupling kit. Kinetic analyses of FcγRI binding were performed according to Ellsworth et al. (16) with some modifications. The running buffer, HBS-EP (10 mM HEPES, 150 mM NaCl, 3 mM EDTA, and 0.005% Surfactant P20 [pH 7.4]) (Biacore), was allowed to flow at 20 μl/min. The injections of FcγRI were performed using the KINJECT mode (volume, 40 μl; dissociation time, 150 s). To regenerate the immobilized proteins, the regeneration buffer (10 mM glycine-HCl [pH 1.8]) was injected for 15 s. Kinetic constants were derived from the sensorgrams using the 1:1 binding model of BIAevaluation software 4.1.

Papain digestion

The papain (Wako) was activated in the buffer (50 mM sodium phosphate/150 mM NaCl [pH 6.0], 1 mM cysteine, 4 mM EDTA, and 1 mg/ml papain) at 37°C for 15 min. Next, 1 mg/ml Ab or Fc-fusion protein was digested with 0.1 mg/ml activated papain in 50 mM sodium phosphate (pH 6.0), 150 mM NaCl, 0.1 mM cysteine, and 4 mM EDTA at 37°C for 24 h.

Results

Purification of soluble human FcRn

FcRn binds to the Fc domain at acidic pH and then releases it at neutral pH. Recombinant soluble hFcRn expressed from CHO cells was purified using a human IgG column by binding at pH 5.8 and releasing at pH 8.1. The fraction purified by the IgG column was electrophoresed at lane 10 of SDS-PAGE gel (Fig. 1*B*). This fraction was then purified using an anion-exchange column with a pH gradient elution. The elution diagram is shown in Fig. 1*A*. Three main peaks were observed. The proteins in these peaks were electrophoresed (Fig. 1*B*) and subjected to Western blot analysis using anti-hFcRn H chain peptide Ab (Fig. 1*C*). Several bands were observed at ~32 kDa in these fractions, and these bands were immunoreactive to anti-hFcRn H chain peptide Ab. These results indicated that the purified FcRn had several isoforms, possibly because of the difference in posttranslational modification, including glycosylation or proteolysis. As shown in Fig. 1*C*, the signals of the higher m.w. bands of hFcRn tend to be weak. There is a possibility that the sugar chain at Asn^{125} of hFcRn interfered with the reactivity of the hFcRn to the anti-hFcRn H chain peptide Ab used. We analyzed the affinity of therapeutic mAbs and Fc fusion proteins to FcRn by SPR using the peak I, II, or III fractions eluted from the anion-exchange column. The K_D values were higher when peak I was used as a ligand in SPR analyses than when peaks II or III were used (data not shown). Because the m.w. of the proteins in peak I was smaller than that in peak II/III and the protein content of peak I varied depending on the lot of the cell culture supernatant, peak I seemed to consist of immature FcRn. The K_D values calculated from the experimental data using peaks II and III were comparable (data not shown). We, therefore, used the main peak (i.e., peak III) in the following experiments.

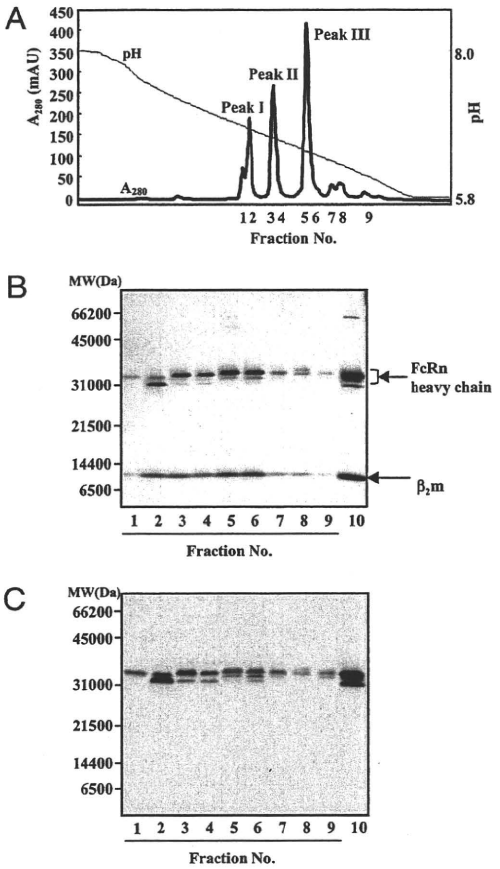

FIGURE 1. Purification and electrophoretic characterization of recombinant human FcRn. *A*, The elution diagram of the anion-exchange chromatography used for the purification of recombinant human FcRn. *B*, SDS-PAGE of the proteins in the fractions indicated in *A*. The protein applied to the anion-exchange column was electrophoresed in *lane 10*. The gel was stained with Imperial protein stain. *C*, Western blot analysis of eluate from the anion-exchange column by anti-hFcRn H chain Ab.

SPR analyses of the affinity between FcRn and Fc domain-containing proteins

Purified FcRn was immobilized onto a CM5 biosensor chip at relatively low densities as described in *Materials and Methods*. Five or six concentrations of Fc domain-containing therapeutic proteins were then injected. Because injection at higher concentrations caused nonspecific binding to flow cells, we analyzed the affinity of therapeutic proteins using sensorgrams obtained at the concentrations at which nonspecific binding was not observed. For example, infliximab was injected at concentrations of 670, 335, 168, 84, and 42 nM, and we analyzed the affinity to FcRn with the bivalent analyte model (Fig. 2). The colored lines were observed sensorgrams, and the black lines were fitting lines generated by the BIAevaluation software. The K_D value (= k_{d1}/k_{a1}) calculated from these sensorgrams was 727 nM. The affinities of adalimumab and etanercept to FcRn were 672 and 3612 nM, respectively (Fig. 2).

The affinities of the 11 kinds of Fc domain-containing proteins to FcRn were measured (Fig. 3). Adalimumab, daclizumab, infliximab, palivizumab, and rituximab were injected at concentrations of 42–670 nM. The concentrations of abatacept, alefacept, and etanercept used were 168–5360 nM, and those of muromonab-CD3, omalizumab, and trastuzumab were 84–1340 nM. Under this condition, the tested therapeutic proteins, except for muromonab-CD3, bound to FcRn. The K_D values measured in our experiments and the serum half-lives in humans reported in the literature are shown in Fig. 3*A*.

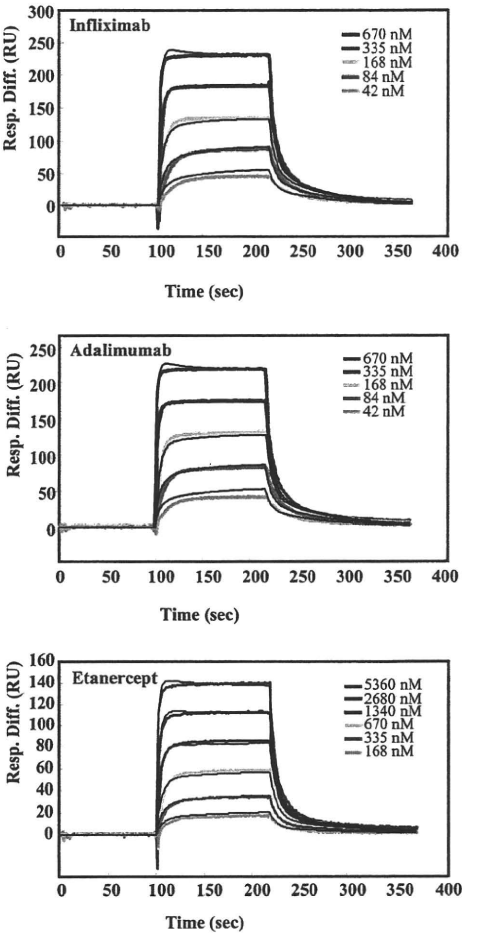

	Infliximab	Adalimumab	Etanercept
k_a1 (1/Ms)	2.09E+05	2.41E+05	3.71E+04
k_d1 (1/s)	0.152	0.162	0.134
k_a2 (1/RUs)	4.56E-05	3.98E-05	3.27E-05
k_d2 (1/s)	9.78E-03	8.80E-03	5.44E-03
Rmax (RU)	3.76E+02	3.47E+02	1.93E+02
Chi2	1.80E+01	1.74E+01	5.37E+00
$K_D=k_d1/k_a1$	**727 nM**	**672 nM**	**3612 nM**

FIGURE 2. Representative sensorgrams of SPR analyses. Infliximab (*upper panel*) or adalimumab (*middle panel*) was injected at concentrations of 42–670 nM and etanercept (*lower panel*) at concentrations of 168–5360 nM. The colored lines are the observed sensorgrams, and the black lines are fitting lines generated by the bivalent analyte model of BIAevaluation software. The association of KINJECT was started at ~100 s, and the dissociation of KINJECT was at ~220 s. The table describes the kinetic values calculated from the sensorgrams of infliximab, adalimumab, and etanercept.

The K_D values and the average values of the serum half-lives are plotted in Fig. 3*B*. The K_D values were closely correlated to the half-lives (contribution ratio = 0.8675) when the results were analyzed after excluding the data for infliximab, rituximab, and trastuzumab (Fig. 3*C*). Concerning infliximab, rituximab, and trastuzumab, which have relatively short half-lives and comparable affinity to other long half-life Abs to FcRn, other critical factor(s) seemed to be involved in regulating their half-lives (see *Discussion*). Although it was impossible to plot the data for mouse mAb muromonab-CD3,

A

Structure	Nonproprietary name	Binding target	Affinity to FcRn K_D (nM)	Half-life (days) cited from the literature	
Human antibody	Adalimumab	TNFα	672	14.7-19.3	Weisman et al., 2003
Humanized antibody	Daclizumab	CD25	846	20	Vincenti et al., 1998
	Omalizumab	IgE	1237	20	Casale et al., 1997
	Palivizumab	RSV F protein	750	19-27	Subramanian et al., 1998
	Trastuzumab	HER2	773	2.7-10	Tokuda et al., 1999
Chimeric antibody	Infliximab	TNFα	727	9.5	Comillie et al., 2001
	Rituximab	CD20	508	9.4	Maloney et al., 1997
Mouse antibody	Muromonab-CD3	CD3	ND	0.75	Hooks et al., 1991
Fc-fusion protein	Abatacept	CD80/CD86	2633	13.1	prescribing information
	Alefacept	CD2	2506	11.3	prescribing information
	Etanercept	TNFα	3612	4	Lee et al., 2003

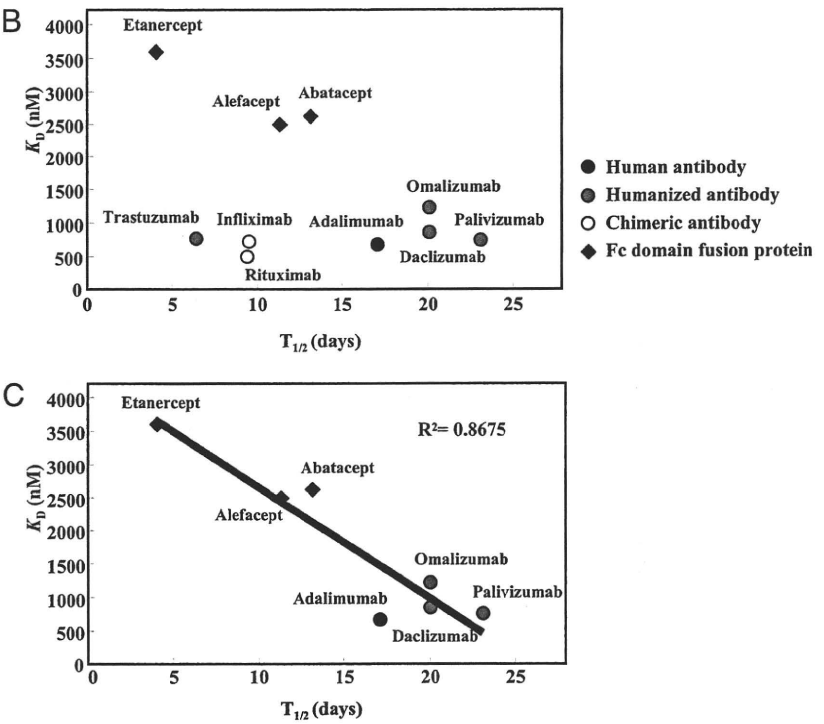

FIGURE 3. K_D values of binding between Fc domain-containing therapeutic proteins and hFcRn and the correlation with their serum half-lives. *A*, The K_D values obtained in our study and the half-lives in humans cited from the literature. The half-life values were obtained from the article reviewed by Lobo et al. (6) [adalimumab (17), daclizumab (18), etanercept (19), infliximab (20), muromonab-CD3 (21), omalizumab (22), palivizumab (23), rituximab (24), and trastuzumab (25)] or from the manufacturer prescribing information. *B*, The graphical presentation of the K_D values and serum half-lives described in *A*. The means of half-lives are plotted on the *x*-axis, and the values of affinity to FcRn are on the *y*-axis. Filled rhombi, Fc domain fusion proteins; closed circle, human Ab; gray circles, humanized Abs; open circle, chimeric Abs. *C*, Regression line of the plots of seven therapeutic proteins. ND, not detected; R^2, coefficient of determination.

which exhibited no significant binding to human FcRn, the half-life of this Ab in humans is the shortest (0.75 d) among the therapeutic proteins examined in this study (21). These results also show the importance of the binding affinity to FcRn in determining the serum half-life. The correlation described above was also observed when other fractions of hFcRn described in Fig. 1 (peaks I and II) were used in SPR analyses (data not shown).

The affinity between FcγRI and Fc domain-containing proteins

Because the affinities of Fc fusion proteins (etanercept, alefacept, and abatacept) to FcRn were lower than those of mAbs, the FcRn-binding region (CH2-CH3 domain interface) of Fc-fusion proteins seems to be structurally different from that of mAbs. We also analyzed the affinity of these proteins to FcγRI to test whether the structural environment around the FcγRI-binding region (hinge proximal region of CH2) is different between Fc-fusion proteins and Abs. Because the regeneration procedure in the SPR assay inactivated FcγRI but not Fc domain-containing therapeutic proteins, therapeutic proteins were immobilized to CM5 biosensor chips, and FcγRI was used as an analyte. The sensorgrams of Fc-fusion proteins (abatacept, alefacept, and etanercept) and mAbs (adalimumab and infliximab) are shown in Fig. 4*A*. The data were analyzed with a 1:1 binding model. The K_D values of the two Fc fusion proteins (alefacept and etanercept) and Abs (adalimumab and infliximab) were comparable (Fig. 4*B*). The K_D values obtained in this study were similar to the data reported for IgG [reviewed by van de Winkel and Anderson (26)]. In contrast, abatacept had a lower affinity to FcγRI. In abatacept, a series of selected mutations those can alter the binding affinity to FcγR were introduced to reduce Fc-mediated cytotoxic effects (Fig. 5) (28, 29). Therefore, the data in Fig. 4 show that the change in the affinity of Fc domain to FcγRI, which is caused by amino acid substitutions, was detected in our experiments. These results suggest that the region interacting with FcγRI (i.e., the hinge proximal region of CH2) was not structurally different between Fc fusion proteins, except for abatacept, and Abs examined.

The affinity between FcRn and Fc domains generated by papain treatment

In Fig. 5, the amino acids sequences of abatacept, alefacept, etanercept, adalimumab, infliximab, and omalizuamb are aligned. The differences in the primary structure of the Fc regions were Glu^{376} and Met^{378} of etanercept, which are attributed to the IgG1 allotype, and Ser^{162}, Ser^{165}, and Ser^{174} of abatacept, which are due

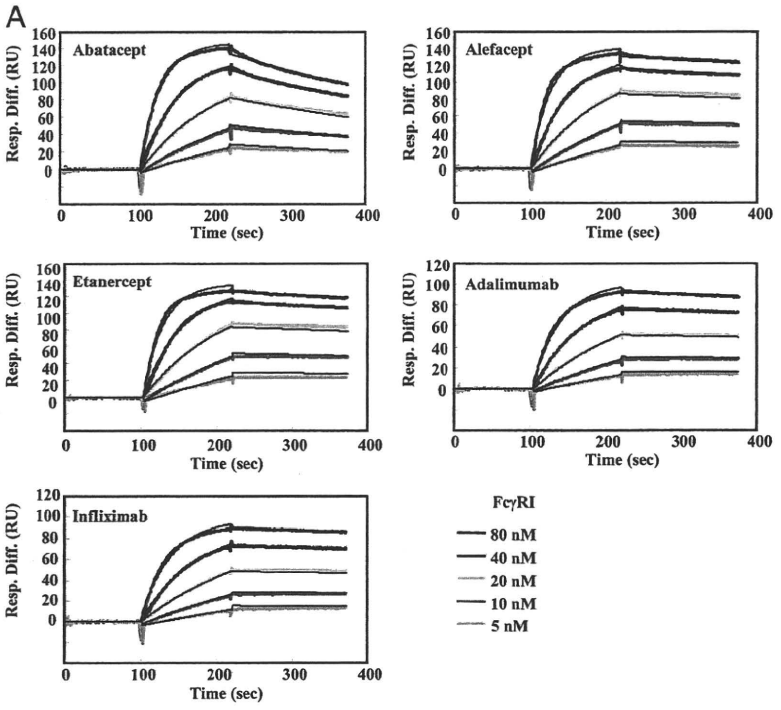

B

	Affinity to FcγRI K_D (nM)
Abatacept	4.82
Alefacept	0.857
Etanercept	0.818
Adalimumab	0.779
Infliximab	0.763

FIGURE 4. The affinity of Fc-fusion proteins and Abs to FcγRI. The Fc-fusion proteins (abatacept, alefacept, and etanercept) and mAbs (adalimumab and infliximab) were immobilized onto CM5 biosensor chips. Recombinant protein of the extracellular domain of FcγRI was injected at concentrations of 5–80 nM and analyzed with a 1:1 binding model (*A*). The colored lines are the observed sensorgrams, and the black lines are fitting lines. Association phase, ~100–220 s; dissociation phase, ~220 s. *B*, The K_D values calculated from the sensorgrams shown in *A*.

to the engineering for decreasing affinity to FcγR and improving protein production (28). To test the possibility that this limited structural difference or posttranscriptional modifications such as glycosylation can give rise to the difference in binding affinity to FcRn, we digested the Fc-fusion proteins or mAbs with papain and analyzed the affinity of their Fc domains to FcRn. The electrophoretic pattern of etanercept and adalimumab digested with papain is shown in Fig. 6*A*. Both etanercept and adalimumab were digested sufficiently for 24 h at 37°C under the conditions described in *Materials and Methods*, whereas digestion was not sufficient after incubating for 2 h. Therefore, the therapeutic proteins digested with papain for 24 h were used for the SPR analyses. The sensorgrams of etanercept (670 nM) and adalimumab (670 nM) were much different without incubation with papain, but they became almost identical after papain digestion (Fig. 6*B*). We measured the affinities to FcRn of five therapeutic proteins (etanercept, alefacept, adalimumab, infliximab, and omalizumab) digested with papain (Fig. 6*C*). Etanercept and alefacept are Fc-fusion proteins with low affinity to FcRn, and omalizumab is an Ab showing lower affinity to FcRn than other Abs. Because it was possible that the proteins were cleaved, in part, into smaller fragments than the Fc domain, the estimated K_D values may have been larger than the actual values. However, it was very clear that the affinities of etanercept, alefacept, infliximab, and omalizumab were increased by papain treatment (Fig. 6*C*).

The affinity of Fc-fusion protein and Abs became comparable after papain digestion, showing that the differences in amino acid sequences or posttranslational modification of the Fc domain did not contribute to the difference in the binding affinity of these proteins to FcRn. It therefore seems likely that the receptor domain of the Fc-fusion protein makes a difference in the higher-order structure of the FcRn-binding region of Fc (i.e., CH2-CH3 interface) or interferes with the binding between Fc domain and FcRn by steric hindrance. Moreover, such a difference or interference seems to be involved in determining the affinity to FcRn for some kinds of Abs, because the K_D values of infliximab and omalizumab were also increased significantly by papain treatment.

The affinity between FcRn and therapeutic proteins binding with target molecules

On the basis of the results suggesting the possibility that another region besides the Fc domain influences the affinity of Fc domain-containing proteins to FcRn, we assumed that binding with the target molecule would also change the affinity to FcRn. Because adalimumab, infliximab, and etanercept bind to the same target molecule, TNF-α, we analyzed the effects of binding with TNF-α on the affinity of these therapeutic proteins to FcRn. First, 0–2680 nM TNF-α was added to 335 nM infliximab and incubated for at least 1 h. The resulting mixture was then injected into the flow cell, and the affinities to FcRn were analyzed. By adding TNF-α, the shape of the sensorgram was drastically altered (Fig. 7*A*). The Abs (adalimumab and infliximab) can maximally bind to two TNF-α trimers, whereas etanercept binds to one TNF-α trimer. When the relative concentrations of TNF-α are low, three molecules of the Ab can bind to each TNF-α trimer, and cross-linked TNF/Ab complexes are formed (30). To evaluate the affinity

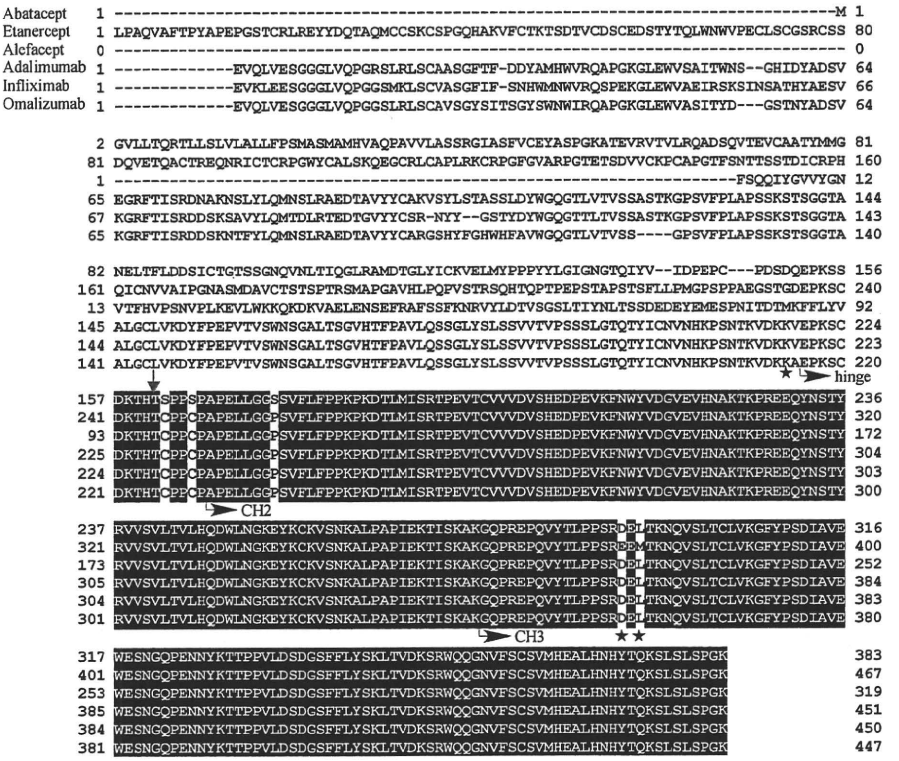

FIGURE 5. The amino acid sequences of abatacept, alefacept, etanercept, and H chains of adalimumab and infliximab. The amino acids marked with a star are different among allotypes of IgG1. The gray arrow is the cleavage site of IgG1 with papain (27). The amino acid sequences were obtained from the following links: abatacept, http://whqlibdoc.who.int/druginfo/18_2_2004_INN91.pdf; alefacept, http://whqlibdoc.who.int/druginfo/DRUG_INFO_14_4_2000_INN-84.pdf; etanercept, http://whqlibdoc.who.int/druginfo/DRUG_INFO_13_2_1999_INN-81.pdf; adalimumab, www.info.pmda.go.jp/shinyaku/g080405/10015900_22000AMX01598_A100_1.pdf; infliximab, www.info.pmda.go.jp/shinyaku/g020102/40031500_21400AMY00013_Q100_2.pdf; and omalizumab, www.drugbank.ca/drugs/DB00043.

between FcRn and TNF-α–binding proteins, excess TNF-α was added to adalimumab, infliximab, and etanercept (8-fold molar excess to 42–670 nM Abs and 4-fold to 168–2680 nM etanercept) to avoid forming nonuniform complexes. The sensorgrams were fitted by the bivalent analyte model (Fig. 7*B*). Although the fitted lines did not completely match the observed sensorgrams, the K_D values of infliximab, adalimumab, and etanercept to FcRn were calculated to be 2057, 1321, and 4286 nM, respectively (Fig. 7*C*). The affinity of infliximab–TNF-α complex or adalimumab–TNF-α complex was lower than that of infliximab or adalimumab, respectively (Fig. 7*C*). These results suggest that at least for these anti–TNF-α Abs, binding with target molecules decreases the affinity to FcRn. They may also suggest that the anti–TNF-α Abs complexed with TNF-α will be degraded more rapidly than anti–TNF-α Abs free from TNF-α in vivo.

Discussion

To our knowledge, this is the first article to elucidate the affinities of clinically used Fc domain-containing therapeutic proteins to FcRn in a comparative study. Because the affinities of these therapeutic proteins to FcRn were found to be highly correlated with the serum half-lives in humans, with the exception of infliximab, rituximab, and trastuzumab, the importance of FcRn in regulating the serum half-life of Fc domain-containing therapeutic proteins was suggested. The key observation was that the Fc-fusion proteins showed lower affinity to FcRn than Abs. These data provided us with one of the answers to the question of why the Fc-fusion proteins containing the Fc domain of human IgG1 exhibit a shorter half-life than human IgG1.

In the current study, we used the bivalent analyte model of BIAevaluation software. Most studies analyzing Fc-FcRn interactions have used the bivalent analyte model (15, 31) or the heterogeneous ligand model (7, 15, 31). Although the sensorgrams in our experiments were able to be fitted by both models, they were better fitted by the bivalent analyte model. Considering that two molecules of hFcRn bind to each IgG, resulting in a 2:1 binding stoichiometry (15), the bivalent analyte model seems to be suitable. It has been reported that the dual bivalent analyte model better fits the data of the FcRn-Fc interaction (32), although there are cases in which the bivalent analyte model does not work well. In the article about the dual bivalent analyte model, it was speculated that high-affinity and low-affinity types of FcRn existed on the surface of the BIAcore chip and that the low-affinity type receptor was probably an experimental artifact (32). Possibly because the content of the low-affinity type of FcRn on the chip is comparatively low in our immobilizing condition, the sensorgrams in our experiments might have been well-fitted by the bivalent analyte model.

Among the therapeutic proteins tested in this study, the Fc fusion proteins showed relatively lower affinities to FcRn (Figs. 2, 3), although the affinities to FcγRI are comparable to those of Abs (Fig. 4). Although the Fc domain binds to FcRn via the CH2-CH3 domain interface (33), the primary structures of the Fc domains of tested therapeutic proteins were almost the same, and cleavage of the Fc domains from Fab or the receptor region gave similar K_D values to FcRn (Fig. 6). These results suggest that the receptor regions of Fc-fusion protein alter the conformation of the FcRn-binding region (CH2-CH3 domain interface), not of the FcγRI-binding region (hinge proximal region of CH2 domain), or cause steric hindrance on the CH2-CH3 domain interface. The influence of regions besides the Fc domain on FcRn-binding regions would also be the case for Abs, as shown in Fig. 7.

Our results presented in this study can provide valuable information regarding the molecular design of novel Fc domain-containing therapeutic proteins and demonstrate the usefulness of FcRn-binding analysis in the characterization of Fc domain-containing therapeutic proteins. In addition to the Fc fusion proteins used in this study, rilonacept, a Fc-fusion protein consisting of ligand-binding domains of the extracellular portions of the human IL-1 receptor component (IL-1RI) and IL-1 receptor accessory protein linked to the Fc portion of human IgG1, and romiplostim,

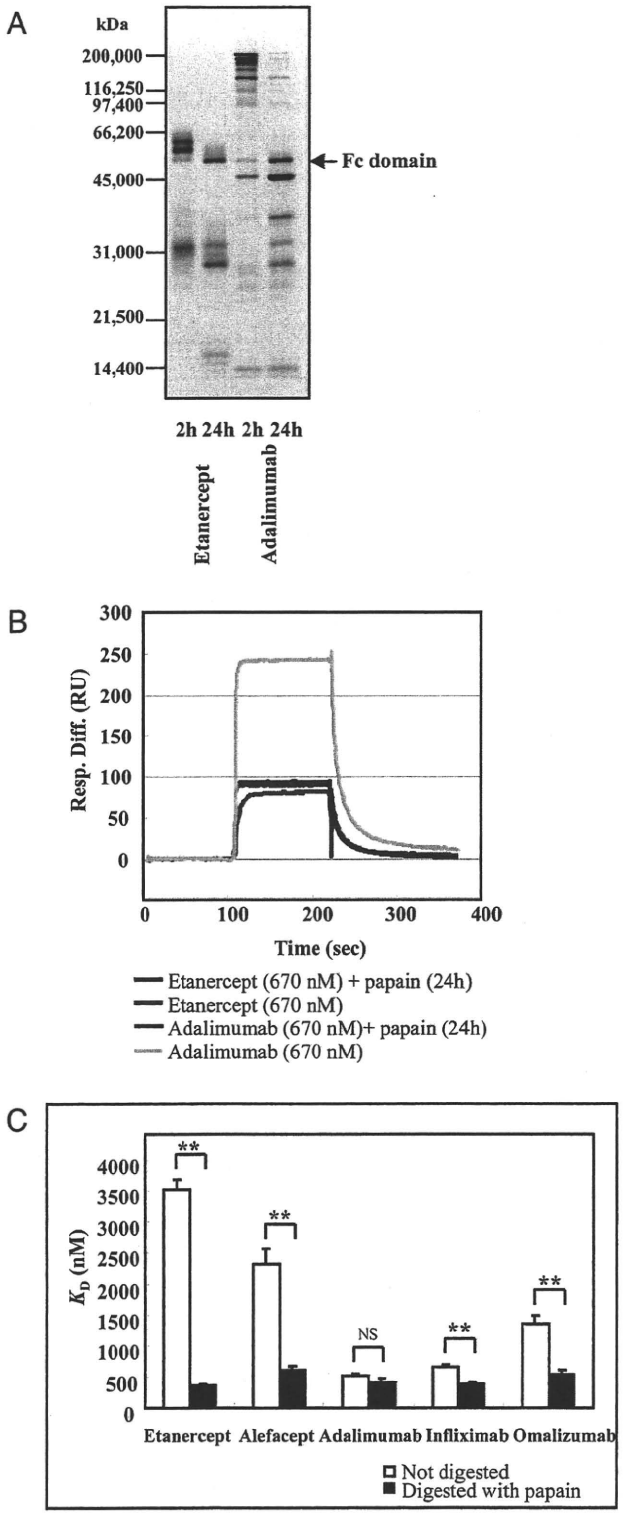

FIGURE 6. Effects of papain digestion on the affinities of Fc domain-containing therapeutic proteins to FcRn. *A*, The nonreduced SDS-PAGE of etanercept and adalimumab digested with papain for 2 and 24 h. *B*, The comparison between the sensorgrams of etanercept and adalimumab with or without papain digestion. *C*, Comparison of the affinity to FcRn among etanercept, alefacept, adalimumab, infliximab, and omalizumab, which were digested or not digested with papain. The K_D values were calculated from the sensorgrams at the range of concentrations described as follows. The concentrations of papain-digested etanercept, papain-digested alefacept, adalimumab, papain-digested adalimumab, infliximab, papain-digested infliximab, and papain-digested omalizumab were 42–670 nM; those of etanercept and alefacept were 168–5360 nM, and those of omalizumab were 42–1340 nM. Each bar shows the average K_D value + SD, which was calculated from three independent experiments. $^{**}p < 0.01$. NS, no significant difference according to Student *t* test.

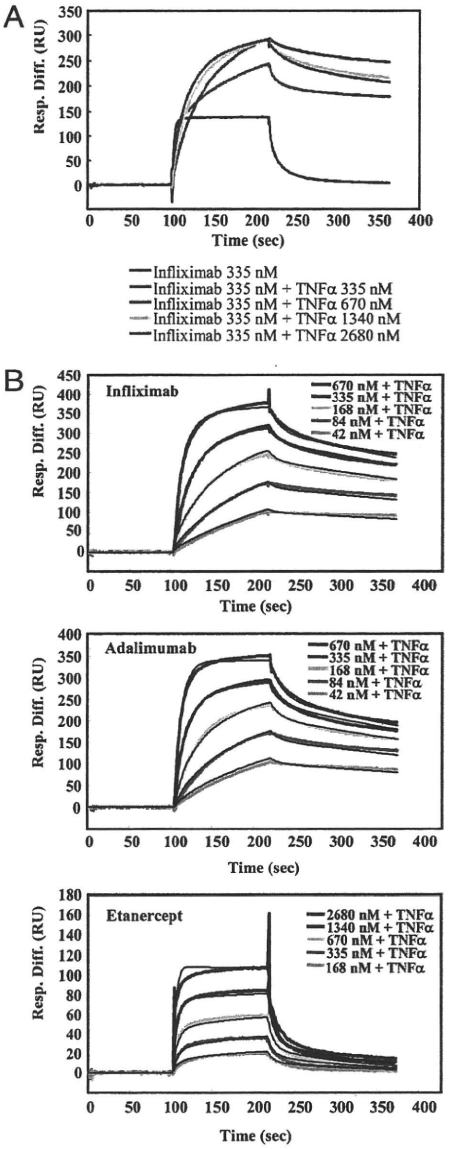

C

	Affinity to FcRn K_D (nM)	
	control	preincubate with TNFα
Etanercept	3705	4286
Adalimumab	673	1321
Infliximab	751	2057

FIGURE 7. Effects of binding with the target molecules on the affinities of Fc domain-containing therapeutic proteins to FcRn. *A*, The sensorgrams of infliximab (335 nM) preincubated with TNF-α (0–2680 nM). *B*, The sensorgrams of infliximab (*upper panel*), adalimumab (*middle panel*), and etanercept (*lower panel*) preincubated with TNF-α (8-fold molar excess to 42–670 nM Abs and 4-fold to 168–2680 nM etanercept). The sensorgrams were fitted by the bivalent analyte model. *C*, The K_D values calculated from the sensorgrams shown in *B*. The values of infliximab, adalimumab, and etanercept derived from the same series of experiments are also shown as controls.

a Fc-peptide fusion protein consisting of human IgG1 Fc domain linked at the C terminus to a peptide containing two thrombopoietin receptor-binding domains, were approved recently (34, 35). The

development of Fc-fusion proteins will receive further attention. Although the Fc domains are used with the intent of prolonging the half-lives of receptor proteins, the half-lives tend not to be fully prolonged to the level of IgG1. It remains unclear whether the receptor regions of Fc-fusion proteins alter the conformation of the CH2-CH3 domain interface or the regions cause steric hindrance on the binding site of FcRn; however, the molecular design of Fc-fusion proteins having a higher affinity to FcRn might be possible in either case.

Reflecting the increasing interest in the development of mAbs and related products, the newly revised guideline for such products was adopted by the European Medicines Agency in 2008 (www.emea.europa.eu/pdfs/human/bwp/15765307enfin.pdf). In the guidelines, it is mentioned that FcRn-binding activity should be provided, as appropriate, in product characterization. Because regions other than the Fc domain might affect the affinity of the protein to FcRn (Figs. 6, 7), the affinity to FcRn should be evaluated as an important quality attribute related to the pharmacokinetic profile, even if the protein has a native Fc domain of IgG1, especially in cases of Fc-fusion proteins. Meanwhile, because it was demonstrated that oxidation of two labile methionines, Met^{252} and Met^{428}, in human IgG1 attenuates binding of the Ab to FcRn (36), alteration of the affinity to FcRn during the production process or storage will reflect structural changes of the protein, including Met oxidation, that will lead to shortening the serum half-life. In addition to IgG, albumin is also known to bind to FcRn in a pH-dependent manner and is protected from degradation (37, 38). The albumin-fusion proteins (e.g., albumin-IFN) or drugs having an albumin-binding moiety are being developed. FcRn-binding characteristics would also be important as a quality attribute of such products, which is related to the pharmacokinetic profile.

As mentioned above, the existence of several Abs having a short half-life and high affinity to FcRn suggested the involvement of other critical factor(s) in regulating the serum half-life of Abs such as trastuzumab, rituximab, or infliximab. Trastuzumab is a humanized Ab directed against human epidermal growth factor receptor 2 (HER2), which is expressed in some types of breast cancer cells. It has been reported that trastuzumab is taken up by HER2-expressing cells via HER2-mediated endocytosis (39, 40). Rituximab, a chimeric Ab directed against CD20, is also internalized in an Ag-mediated manner (41). Because the ligand-dependent internalization is followed by degradation of Abs, this property seems to be an important reason for the short half-life of trastuzumab and rituximab. It has been reported that, in general, the half-life of monoclonal IgG Abs increases depending on the degree of humanization in the order of murine < chimeric < humanized < human (6, 41, 42). Because infliximab and rituximab are chimeric Abs, the involvement of common factors influencing the half-life of chimeric Abs such as the presence of human anti-chimeric Ab would be another reason for the shorter half-life.

As shown in Fig. 7, the affinities of infliximab–TNF-α complex and adalimumab–TNF-α complex seemed to be lower than those of infliximab and adalimumab. If the affinity of therapeutic proteins/target molecules complexes to FcRn is lower than that of the free therapeutic proteins, the complexes will be degraded faster. Therefore, the half-lives of such therapeutic proteins seem to be shortened in the case that the target molecules are abundant in the bodies of patients. In contrast, if the affinity to FcRn of therapeutic proteins/target molecule complexes is higher than that of the free drugs, the complexes of drug and target molecules will have longer half-lives than free drugs. Because there are many factors affecting the elimination of Abs [reviewed by Tabrizi et al. (41)], further studies are necessary to elucidate the critical factors impacting the half-lives of Fc domain-containing proteins, in addition to the affinity to FcRn. Binding characteristics of the Fc domain-containing proteins or their complex with target molecules to FcγRs would be one of the important issues to be examined in regard to the impact on their elimination.

In conclusion, we showed the importance of the affinity to FcRn in determining the serum half-life of Fc domain-containing therapeutic proteins. Further investigation regarding the molecular structures that regulate the affinity of the engineered protein to FcRn will accelerate the development of therapeutic proteins with a desired half-life.

Acknowledgments

We thank Dr. Pamela Bjorkman for the gift of the cell line expressing FcRn.

Disclosures

The authors have no financial conflicts of interest.

References

1. Morell, A., W. D. Terry, and T. A. Waldmann. 1970. Metabolic properties of IgG subclasses in man. *J. Clin. Invest.* 49: 673–680.
2. Simister, N. E., and K. E. Mostov. 1989. An Fc receptor structurally related to MHC class I antigens. *Nature* 337: 184–187.
3. Junghans, R. P., and C. L. Anderson. 1996. The protection receptor for IgG catabolism is the β_2-microglobulin-containing neonatal intestinal transport receptor. *Proc. Natl. Acad. Sci. USA* 93: 5512–5516.
4. Ghetie, V., S. Popov, J. Borvak, C. Radu, D. Matesoi, C. Medesan, R. J. Ober, and E. S. Ward. 1997. Increasing the serum persistence of an IgG fragment by random mutagenesis. *Nat. Biotechnol.* 15: 637–640.
5. Raghavan, M., V. R. Bonagura, S. L. Morrison, and P. J. Bjorkman. 1995. Analysis of the pH dependence of the neonatal Fc receptor/immunoglobulin G interaction using antibody and receptor variants. *Biochemistry* 34: 14649–14657.
6. Lobo, E. D., R. J. Hansen, and J. P. Balthasar. 2004. Antibody pharmacokinetics and pharmacodynamics. *J. Pharm. Sci.* 93: 2645–2668.
7. Datta-Mannan, A., D. R. Witcher, Y. Tang, J. Watkins, and V. J. Wroblewski. 2007. Monoclonal antibody clearance: impact of modulating the interaction of IgG with the neonatal Fc receptor. *J. Biol. Chem.* 282: 1709–1717.
8. Vaccaro, C., J. Zhou, R. J. Ober, and E. S. Ward. 2005. Engineering the Fc region of immunoglobulin G to modulate in vivo antibody levels. *Nat. Biotechnol.* 23: 1283–1288.
9. Hinton, P. R., J. M. Xiong, M. G. Johlfs, M. T. Tang, S. Keller, and N. Tsurushita. 2006. An engineered human IgG1 antibody with longer serum half-life. *J. Immunol.* 176: 346–356.
10. Dall'Acqua, W. F., P. A. Kiener, and H. Wu. 2006. Properties of human IgG1s engineered for enhanced binding to the neonatal Fc receptor (FcRn). *J. Biol. Chem.* 281: 23514–23524.
11. Petkova, S. B., S. Akilesh, T. J. Sproule, G. J. Christianson, H. Al Khabbaz, A. C. Brown, L. G. Presta, Y. G. Meng, and D. C. Roopenian. 2006. Enhanced half-life of genetically engineered human IgG1 antibodies in a humanized FcRn mouse model: potential application in humorally mediated autoimmune disease. *Int. Immunol.* 18: 1759–1769.
12. Yeung, Y. A., M. K. Leabman, J. S. Marvin, J. Qiu, C. W. Adams, S. Lien, M. A. Starovasnik, and H. B. Lowman. 2009. Engineering human IgG1 affinity to human neonatal Fc receptor: impact of affinity improvement on pharmacokinetics in primates. *J. Immunol.* 182: 7663–7671.
13. Nissim, A., and Y. Chernajovsky. 2008. Historical development of monoclonal antibody therapeutics. In *Therapeutic Antibodies (Handbook of Experimental Pharmacology)*, Vol. 181. Y. Chernajovsky and A. Nissim eds. Springer, New York, p. 3–18.
14. Reichert, J. M., C. J. Rosensweig, L. B. Faden, and M. C. Dewitz. 2005. Monoclonal antibody successes in the clinic. *Nat. Biotechnol.* 23: 1073–1078.
15. West, A. P., Jr., and P. J. Bjorkman. 2000. Crystal structure and immunoglobulin G binding properties of the human major histocompatibility complex-related Fc receptor. *Biochemistry* 39: 9698–9708.
16. Ellsworth, J. L., M. Maurer, B. Harder, N. Hamacher, M. Lantry, K. B. Lewis, S. Rene, K. Byrnes-Blake, S. Underwood, K. S. Waggie, et al. 2008. Targeting immune complex-mediated hypersensitivity with recombinant soluble human FcγRIA (CD64A). *J. Immunol.* 180: 580–589.
17. Weisman, M. H., L. W. Moreland, D. E. Furst, M. E. Weinblatt, E. C. Keystone, H. E. Paulus, L. S. Teoh, R. B. Velagapudi, P. A. Noertersheuser, G. R. Granneman, et al. 2003. Efficacy, pharmacokinetic, and safety assessment of adalimumab, a fully human anti-tumor necrosis factor-α monoclonal antibody, in adults with rheumatoid arthritis receiving concomitant methotrexate: a pilot study. *Clin. Ther.* 25: 1700–1721.
18. Vincenti, F., R. Kirkman, S. Light, G. Bumgardner, M. Pescovitz, P. Halloran, J. Neylan, A. Wilkinson, H. Ekberg, R. Gaston, et al. 1998. Interleukin-2-receptor blockade with daclizumab to prevent acute rejection in renal transplantation. *N. Engl. J. Med.* 338: 161–165.
19. Lee, H., H. C. Kimko, M. Rogge, D. Wang, I. Nestorov, and C. C. Peck. 2003. Population pharmacokinetic and pharmacodynamic modeling of etanercept using logistic regression analysis. *Clin. Pharmacol. Ther.* 73: 348–365.

20. Cornillie, F., D. Shealy, G. D'Haens, K. Geboes, G. Van Assche, J. Ceuppens, C. Wagner, T. Schaible, S. E. Plevy, S. R. Targan, and P. Rutgeerts. 2001. Infliximab induces potent anti-inflammatory and local immunomodulatory activity but no systemic immune suppression in patients with Crohn's disease. *Aliment. Pharmacol. Ther.* 15: 463–473.
21. Hooks, M. A., C. S. Wade, and W. J. Millikan, Jr. 1991. Muromonab CD-3: a review of its pharmacology, pharmacokinetics, and clinical use in transplantation. *Pharmacotherapy* 11: 26–37.
22. Casale, T. B., I. L. Bernstein, W. W. Busse, C. F. LaForce, D. G. Tinkelman, R. R. Stoltz, R. J. Dockhorn, J. Reimann, J. Q. Su, R. B. Fick, Jr., and D. C. Adelman. 1997. Use of an anti-IgE humanized monoclonal antibody in ragweed-induced allergic rhinitis. *J. Allergy Clin. Immunol.* 100: 110–121.
23. Subramanian, K. N., L. E. Weisman, T. Rhodes, R. Ariagno, P. J. Sánchez, J. Steichen, L. B. Givner, T. L. Jennings, F. H. Top, Jr., D. Carlin, and E. Connor. 1998. Safety, tolerance and pharmacokinetics of a humanized monoclonal antibody to respiratory syncytial virus in premature infants and infants with bronchopulmonary dysplasia; MEDI-493 Study Group. *Pediatr. Infect. Dis. J.* 17: 110–115.
24. Maloney, D. G., A. J. Grillo-López, C. A. White, D. Bodkin, R. J. Schilder, J. A. Neidhart, N. Janakiraman, K. A. Foon, T. M. Liles, B. K. Dallaire, et al. 1997. IDEC-C2B8 (Rituximab) anti-CD20 monoclonal antibody therapy in patients with relapsed low-grade non-Hodgkin's lymphoma. *Blood* 90: 2188–2195.
25. Tokuda, Y., T. Watanabe, Y. Omuro, M. Ando, N. Katsumata, A. Okumura, M. Ohta, H. Fujii, Y. Sasaki, T. Niwa, and T. Tajima. 1999. Dose escalation and pharmacokinetic study of a humanized anti-HER2 monoclonal antibody in patients with HER2/neu-overexpressing metastatic breast cancer. *Br. J. Cancer* 81: 1419–1425.
26. van de Winkel, J. G., and C. L. Anderson. 1991. Biology of human immunoglobulin G Fc receptors. *J. Leukoc. Biol.* 49: 511–524.
27. Wenig, K., L. Chatwell, U. von Pawel-Rammingen, L. Björck, R. Huber, and P. Sondermann. 2004. Structure of the streptococcal endopeptidase IdeS, a cysteine proteinase with strict specificity for IgG. *Proc. Natl. Acad. Sci. USA* 101: 17371–17376.
28. Davis, P. M., R. Abraham, L. Xu, S. G. Nadler, and S. J. Suchard. 2007. Abatacept binds to the Fc receptor CD64 but does not mediate complement-dependent cytotoxicity or antibody-dependent cellular cytotoxicity. *J. Rheumatol.* 34: 2204–2210.
29. Presta, L. G. 2008. Molecular engineering and design of therapeutic antibodies. *Curr. Opin. Immunol.* 20: 460–470.
30. Scallon, B., A. Cai, N. Solowski, A. Rosenberg, X. Y. Song, D. Shealy, and C. Wagner. 2002. Binding and functional comparisons of two types of tumor necrosis factor antagonists. *J. Pharmacol. Exp. Ther.* 301: 418–426.
31. Martin, W. L., and P. J. Bjorkman. 1999. Characterization of the 2:1 complex between the class I MHC-related Fc receptor and its Fc ligand in solution. *Biochemistry* 38: 12639–12647.
32. Gurbaxani, B. M., and S. L. Morrison. 2006. Development of new models for the analysis of Fc-FcRn interactions. *Mol. Immunol.* 43: 1379–1389.
33. Martin, W. L., A. P. West, Jr., L. Gan, and P. J. Bjorkman. 2001. Crystal structure at 2.8 A of an FcRn/heterodimeric Fc complex: mechanism of pH-dependent binding. *Mol. Cell* 7: 867–877.
34. Osborne, R. 2009. Fresh from the biologic pipeline. *Nat. Biotechnol.* 27: 222–225.
35. Cines, D. B., U. Yasothan, and P. Kirkpatrick. 2008. Romiplostim. *Nat. Rev. Drug Discov.* 7: 887–888.
36. Pan, H., K. Chen, L. Chu, F. Kinderman, I. Apostol, and G. Huang. 2009. Methionine oxidation in human IgG2 Fc decreases binding affinities to protein A and FcRn. *Protein Sci.* 18: 424–433.
37. Chaudhury, C., S. Mehnaz, J. M. Robinson, W. L. Hayton, D. K. Pearl, D. C. Roopenian, and C. L. Anderson. 2003. The major histocompatibility complex-related Fc receptor for IgG (FcRn) binds albumin and prolongs its lifespan. *J. Exp. Med.* 197: 315–322.
38. Chaudhury, C., C. L. Brooks, D. C. Carter, J. M. Robinson, and C. L. Anderson. 2006. Albumin binding to FcRn: distinct from the FcRn-IgG interaction. *Biochemistry* 45: 4983–4990.
39. Steinhauser, I., B. Spänkuch, K. Strebhardt, and K. Langer. 2006. Trastuzumab-modified nanoparticles: optimisation of preparation and uptake in cancer cells. *Biomaterials* 27: 4975–4983.
40. Wuang, S. C., K. G. Neoh, E. T. Kang, D. W. Pack, and D. E. Leckband. 2008. HER-2-mediated endocytosis of magnetic nanospheres and the implications in cell targeting and particle magnetization. *Biomaterials* 29: 2270–2279.
41. Tabrizi, M. A., C. M. Tseng, and L. K. Roskos. 2006. Elimination mechanisms of therapeutic monoclonal antibodies. *Drug Discov. Today* 11: 81–88.
42. Kuester, K., and C. Kloft. 2006. Pharmacokinetics of monoclonal antibodies. In *Pharmacokinetics and Pharmacodynamics of Biotech Drugs*. B. Meibohm, ed. Wiley-VCH Verlag, Weinheim, Germany, p. 45–91.

Division of Drugs, National Institute of Health Sciences, Japan

Ammonium ion level in serum affects doxorubicin release from liposomes

H. SHIBATA, H. SAITO, C. YOMOTA, T. KAWANISHI

Received July 30, 2009, accepted September 14, 2009

Hiroko Shibata, Ph.D., National Institute of Health Science, Kamiyoga 1-18-1, Setagaya-ku, Tokyo 158-8501, Japan
h-shibata@nihs.go.jp

Pharmazie 65: 251–253 (2010) *doi: 10.1691/ph.2010.9255*

In this study, we measured the release of drug from liposome-encapsulated doxorubicin (DXR) in human and mouse serum. While human serum did not induce DXR-release, mouse serum significantly induced DXR-release in a temperature- and time-dependent manner. Release of DXR was clearly observed in ultrafiltrated mouse serum, indicating that low-molecular substances affect DXR-release. Therefore, the level of Na^+, Cl^-, NH_4^+, and urea nitrogen in each type of serum was measured. Only the concentration of NH_4^+ in mouse serum was significantly higher than that in human serum. Furthermore, addition of ammonium acetate to human serum induced DXR release at the same level observed in mouse serum. These results indicate that the NH_4^+ concentration in serum might greatly affect the release of DXR from liposomes.

1. Introduction

Recently, various liposomal products have been developed and applied to clinical treatment (Coukell and Brogden 1998; Maurer et al. 2001). It is a global requirement that evaluation standards for liposomal products are established to ensure their quality (Burgess et al. 2002). The main purpose of using liposomalization is to stabilize drugs *in vivo* and to control release. For example, the serum half-life of DOXIL®, which is the antitumor agent doxorubicin (DXR) encapsulated in a PEGylated or so-called 'stealth' liposome, is about 90 h (Fujisaka et al. 2006), while that of injected DXR is less than 1 h (Mross et al. 1988). Therefore, drug release (or leakage) is one of the most important formulation properties of liposomal products for quality assessment. *In vitro* drug-release tests for appropriately measuring drug release from liposomes would be very useful for assessing lot-to-lot variability or the release characteristics of liposome products. At present, however, few studies have examined how we should assess *in vitro* drug-release appropriately. From this standpoint, we have studied whether or not an *in vitro* release test, which is related to *in vivo* stability, can be established. It's preferable that such an in vitro drug-release test is based on the *in vivo* release mechanism and correlates with the *in vivo* release profiles. In order to achieve *in vivo* relevance, drug release should be measured under conditions that are as near as possible to the physiological condition. Thus, as a first step, we have investigated the utility of human or mouse serum in the assessment of DXR release from stealth liposome-encapsulated DXR (DXR-SL).

2. Investigations, results and discussion

DXR-SL were incubated with mouse or human serum at various temperatures (37, 45, or 52 °C), and the ratio of DXR release was measured. As a result, mouse serum induced significant DXR release from DXR-SL in a temperature- and time-dependent manner (Fig. 1). In the case of human serum, however, the DXR-release rate was extremely low, even at 52 °C. To our knowledge, it has not been reported that drug release from liposomes differs greatly between human serum and mouse serum.

To elucidate this difference, DXR release from DXR-SL was measured in the filtrate of each serum after ultrafiltration (3 kDa or 10 kDa cut-off). Ultrafiltrated mouse serum induced significant DXR release, although it was slightly lower than that in unfiltered serum (Fig. 2A). In human serum, the DXR-release rate in the filtrate was also slightly lower than that in unfiltered serum. This result indicates that low molecular substances largely affect the release of DXR induced in mouse serum. When DXR-SL was incubated with rat or bovine serum, in addition to human and mouse serum, only mouse serum induced DXR release from DXR-SL (Fig. 2B). Next, we compared the DXR-release rate in four kinds of serum: two kinds of fresh serum collected from CD-1 mice and BALB/c mice (prepared in our laboratory), commercial mouse serum that had been used in the above tests, and human serum. As a result, significant DXR release was observed in only the commercial mouse serum, while the DXR-release rate in fresh mouse serum was equivalent to that in human serum (Fig. 2C). These results indicate the possibility that the low molecular substances affecting drug release are specific to the commercial mouse serum.

Therefore, we measured the concentration of typical low molecular substances in blood, such as Na^+, Cl^-, NH_4^+ and urea nitrogen, in each type of serum. Surprisingly, the NH_4^+ level of the commercial mouse serum was 100-fold higher than that of human serum (Fig. 3A). Likewise, the NH_4^+ level was significantly high in another commercially available mouse serum. On the other hand, the concentration of urea nitrogen in the commercial mouse serum was one-twentieth of that in human serum. The concentration of sodium or chloride was normal in all serum. Next, we examined the effect of NH_4^+ level on DXR release from DXR-SL. It was expected that the pH of the commercial mouse serum would be higher than that of human serum. However, there were no differences in pH between mouse and human serum (data not shown). Thus, we added ammonium

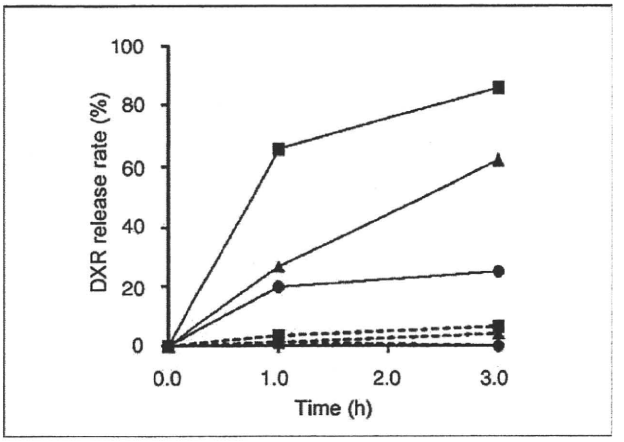

Fig. 1: DXR-release rate in mouse or human serum. DXR-SL (DXR 200 μg/ml) was incubated in human (dashed line) or mouse (solid line) serum (final 90% (v/v)) at 37 °C (circle), 45 °C (triangle), or 52 °C (square) for indicated time

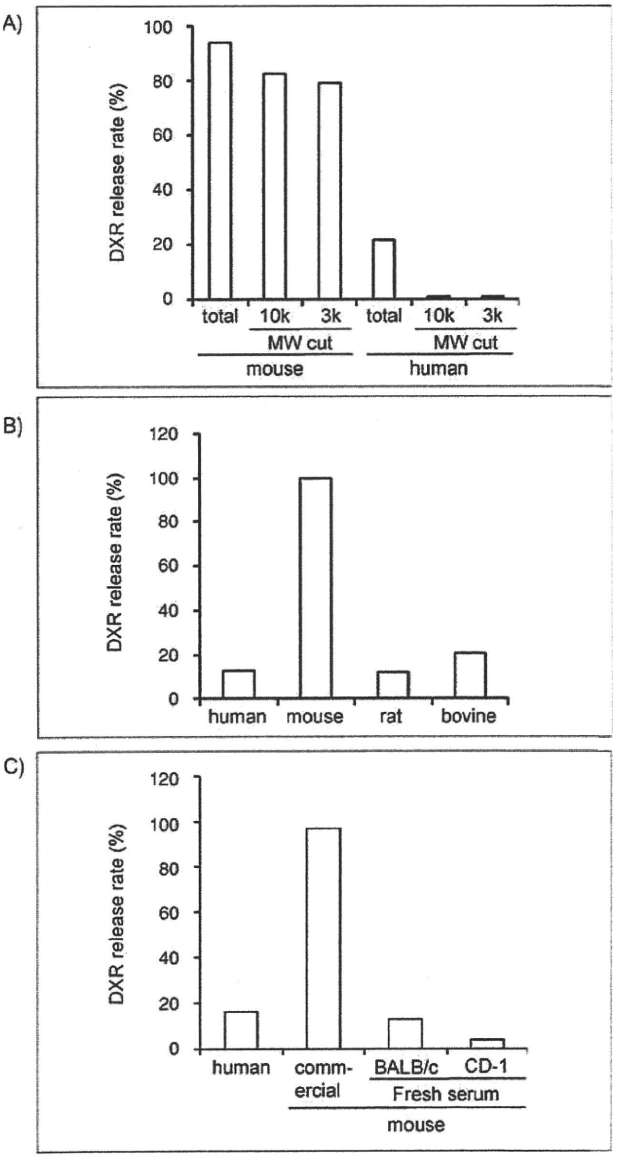

Fig. 2: Effect of difference in serum on DXR-release. A) Effect of ultrafiltrated serum on the DXR-release rate. DXR-SL (DXR 200 μg/ml) was incubated in the filtrate (final 90% (v/v)) for 3 h at 52 °C. DXR-release rate in rat and bovine serum B), and fresh mouse serum collected from BALB/c and CD-1 mice C), in addition to human and mouse serum, were measured after incubation for 3h at 52 °C

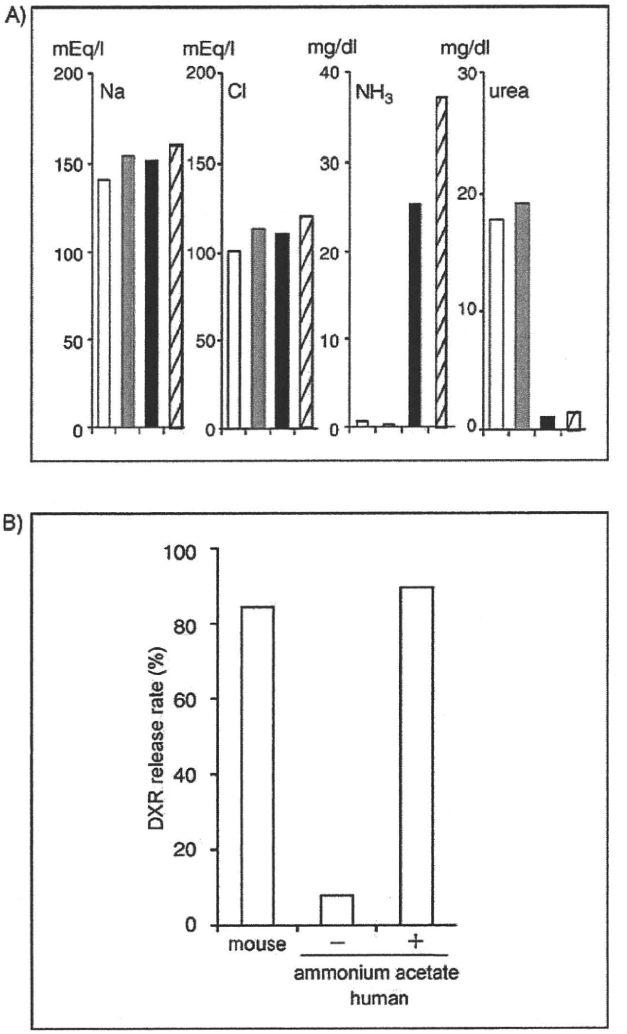

Fig. 3: NH_4^+ level affects DXR release. A) Na^+, Cl^-, NH_4^+ and urea nitrogen in human (white column), fresh mouse serum (gray column), commercial mouse serum (black and shaded column) were measured. B) Ammonium acetate was added to human serum at a final concentration of 1.34 mg/ml which is almost same as the NH_4^+ level in mouse serum. The DXR-release rate in this modified human serum was measured as described in Fig. 1

acetate solution to human serum to the same NH_4^+ level in commercial mouse serum without changing the pH, and measured the DXR-release rate in the adjusted human serum. As in mouse serum, significant DXR release was observed in human serum with ammonium acetate (Fig. 3B). These results suggest that the high NH_4^+ level is one of the causes of the high DXR-release rate in commercial mouse serum.

It is unclear why the NH_4^+ level is markedly increased in commercial mouse serum. Commonly, the blood NH_4^+ level should be measured immediately after blood drawing and centrifugation. Hemolysis and leaving the samples as whole blood at room temperature are causes for elevated test values (Howanitz et al. 1984; Lindner and Bauer 1993). AMP deaminase in red blood cells catalyzes the production of ammonia from protein and amino acids (Nathans et al. 1978). Although we did not investigate the effects in full, we found that, even in human serum, repeating freeze-thaw cycles and long storage tended to increase the DXR-release rate (data not shown). Thus, the high NH_4^+ may be due to a delay in collecting serum after blood drawing, hemolysis, repeating freeze-thaw cycles, or long storage. It is important to stress, however, that the commercial mouse serum used in our examinations is fully compatible with immune assays, such as ELISA or immunostaining, for which it is generally used.

DXR is encapsulated in liposomes by a remote loading method based on the gradient of ammonium sulfate. The mechanism of accumulation is believed to be as follows (Haran et al. 1993). Removal of ammonium sulfate from the extraliposomal medium of liposomes creates an ammonium sulfate gradient $[(NH_4)_2SO_4]_{lip.} > [(NH_4)_2SO_4]_{med.}$ The very high permeability coefficient of neutral NH_3 leads to fast diffusion of NH_3 into the extraliposomal medium. For every NH_3 molecule that leaves the liposome, one proton is left behind, forming a pH gradient across the liposomal membrane. Because DXR is a weakly basic compound (pKa = 8.25), nonionic DXR in the extraliposomal medium diffuses through the lipid bilayer, is protonated and trapped as an ionic form, and accumulates in the intraliposomal aqueous phase by forming a precipitate with sulfate ions. The process can be summarized as an exchange between NH_3 efflux and DXR influx. Therefore, the addition of high concentration ammonium salt to the extraliposomal phase of DXR-SL may induce NH_3 influx into intraliposomes. As a result, the intraliposomal pH may be elevated, and nonionic DXR may diffuse out through the lipid bilayer of liposomes. While the details of the mechanism remain to be elucidated, we speculate that the significant DXR release from DXR-SL in the commercial mouse serum could be caused by high NH_4^+ levels in this way.

Our data revealed that 1) there was almost no DXR release from DXR-SL in human serum, while mouse serum induced significant DXR release; 2) the high NH_4^+ level in mouse serum, especially in commercial mouse serum, is one of the factors leading to the markedly high DXR-release rate; and 3) the concentration of NH_4^+ in the test solution can greatly affect the release of DXR from DXR-SL. Thus, if serum or plasma is used for an *in vitro* drug-release test of liposomal products that are prepared by ammonium sulfate gradient, it will be necessary to control both the lot and the storage period.

3. Experimental

3.1. Materials

Hydrogenated soy phosphatidylcholine (HSPC) and (N-(carbonyl-methoxy polyethyleneglycol 2000)-1,2-distearoyl-sn-glycero-3-phosphoethanolamine (DSPE-PEG2000) were purchased from Nippon Oil and Fat (Tokyo, Japan). Cholesterol (Chol) was of analytical grade (Wako Pure Chemical, Osaka, Japan). Adriacin® injection 10 (Kyowa Hakko Kirin Co., Ltd.), which is doxorubicin (DXR) injection, was purchased from a general sales agency for drugs in Japan. Mouse, rat serum (Valley Biomedical, Inc., VA), and human serum (Biopredic International, Rennes, France) were obtained from KAC Co., Ltd. (Kyoto, Japan). Another mouse serum was obtained from Cedarlane Laboratories Limited (Ontario, Canada). Bovine serum was purchased from Invitrogen (Carlsbad, CA). Fresh mouse serum collected from CD-1 mice was supplied by Charles River (Kanagawa, Japan). Sepharose CL-4B and Sephadex G-25 prepacked columns, PD-10 Desalting Columns, were purchased from GE Healthcare Japan (Tokyo, Japan).

3.2. Liposome preparation

DXR-SL composed of HSPC/Chol/DSPE-PEG2000 (56.5/38/5.4 molar ratio) was prepared by a modified ethanol injection method (Maitani et al. 2001). DXR was encapsulated into liposomes by remote loading using an ammonium sulfate gradient (Lasic et al. 1992). Briefly, all lipids were dissolved in about 5 ml of ethanol, and the ethanol was removed with a rotary evaporator leaving behind about 1 ml of the ethanol solution. Next, 4 ml of 300 mM ammonium sulfate was added to the ethanol solution. Liposomes formed spontaneously after further evaporation of the residual ethanol. After five freeze-thaw cycles, liposomes were extruded through a series of polycarbonate filters (Nucleopore, CA) with pore sizes ranging from 0.4 to 0.1 μm. The mean diameter of resulting liposomes was determined by dynamic light scattering using a DLS-7000 (Otsuka Electronics Co. Ltd., Osaka, Japan). The diameter of extruded liposomes was in the range of 110 ± 30 nm. Following extrusion, liposomes were ultracentrifuged at 80,000 rpm for 45 min at 4 °C, and suspended in normal saline. The concentration of phospholipid was determined by colorimetric assay using Phopholipids C (Wako Pure Chemical Industries, Ltd., Osaka, Japan). DXR was added to the liposomes at a DXR/liposome ratio of 0.2:1 (w/w), and liposomes were incubated for 1 h at 55 °C. The liposome-encapsulated DXR, DXR-SL, was exchanged by eluting through a PD-10 Desalting Column equilibrated with normal saline.

3.3. Release of doxorubicin

DXR-SL (DXR 200 μg/ml) was incubated in each serum (final 90% (v/v)) for indicated time at 37, 45 or 52 °C. After incubation, samples were passed through a Sepharose CL-4B column equilibrated with normal saline to separate the liposomal DXR from serum protein and free drug. The fraction of liposomal DXR was mixed with an equal volume of hydrochloric acid/isopropanol, and the fluorescent intensity was read at 590 nm (excitation 470 nm). The release rate was calculated from the amount of liposomal-DXR. For ultrafiltration, 4 ml of each serum was ultrafiltrated on centrifugal filter units (NMWL 10k or 3k, AmiconUltra, Millipore Corporate Headquarters, Billerica, MA), and 2 ml filtrate was used for release assay. Ammonium acetate was dissolved in water (134 mg/mL) and added to human serum at a final concentration of 1.34 mg/mL which is almost same as the NH_4^+ level in mouse serum.

3.4. Ion levels in serum

Measurement of Na^+, Cl^-, NH_4^+ and urea nitrogen in each serum was outsourced to the Mitsubishi Chemical Medience Corporation (Tokyo, Japan). Na^+ and Cl^- were measured by electrode method. NH_4^+ and urea nitrogen were measured by indophenol colorimetric method (Fujii-Okuda method) and urease-LEDH method, respectively.

Acknowledgements: We thank Dr. Nakashima, Pharmaceutical R&D Division, Janssen Pharmaceutical K.K., for providing critical comments. We also thank Professor Maitani, Hoshi University, Professor Mruyama and Dr. Suzuki, Teikyo University, for advices regarding the preparation of stealth liposome. The present study was supported by the Japan Health Sciences Foundation (KHB1006).

References

Burgess DJ, Hussain AS, Ingallinera TS, Chen ML (2002) Assuring quality and performance of sustained and controlled release parenterals: AAPS workshop report, co-sponsored by FDA and USP. Pharm Res 19: 1761–1768.

Coukell AJ, Brogden RN (1998) Liposomal amphotericin B. Therapeutic use in the management of fungal infections and visceral leishmaniasis. Drugs 55: 585–612.

Fujisaka Y, Horiike A, Shimizu T, Yamamoto N, Yamada Y, Tamura T (2006) Phase 1 clinical study of pegylated liposomal doxorubicin (JNS002) in Japanese patients with solid tumors. Jpn J Clin Oncol 36: 768–774.

Haran G, Cohen R, Bar LK, Barenholz Y (1993) Transmembrane ammonium sulfate gradients in liposomes produce efficient and stable entrapment of amphipathic weak bases. Biochim Biophys Acta 1151: 201–215.

Howanitz JH, Howanitz PJ, Skrodzki CA, Iwanski JA (1984) Influences of specimen processing and storage conditions on results for plasma ammonia. Clin Chem 30: 906–908.

Lasic DD, Frederik PM, Stuart MC, Barenholz Y, McIntosh TJ (1992) Gelation of liposome interior. A novel method for drug encapsulation. FEBS Lett 312: 255–258.

Lindner A, Bauer S (1993) Effect of temperature, duration of storage and sampling procedure on ammonia concentration in equine blood plasma. Eur J Clin Chem Clin Biochem 31: 473–476.

Maitani Y, Soeda H, Junping W, Takayama K (2001) Modified ethanol injection method for liposomes containing beta-sitosterol beta-d-glucoside. J Liposome Res 11: 115–125.

Maurer N, Fenske DB, Cullis PR (2001) Developments in liposomal drug delivery systems. Expert Opin Biol Ther 1: 923–947.

Mross K, Maessen P, van der Vijgh WJ, Gall H, Boven E, Pinedo HM (1988) Pharmacokinetics and metabolism of epidoxorubicin and doxorubicin in humans. J Clin Oncol 6: 517–526.

Nathans GR, Chang D, Deuel TF (1978) AMP deaminase from human erythrocytes. Methods Enzymol 51: 497–502.

Journal of Chromatography B, 878 (2010) 1466–1470

Contents lists available at ScienceDirect

Journal of Chromatography B

journal homepage: www.elsevier.com/locate/chromb

Analysis of intracellular doxorubicin and its metabolites by ultra-high-performance liquid chromatography

Kumiko Sakai-Kato*, Eiko Saito, Keiko Ishikura, Toru Kawanishi

Division of Drugs, National Institute of Health Sciences, 1-18-1 Kamiyoga, Setagaya-ku, Tokyo 158-8501, Japan

ARTICLE INFO

Article history:
Received 28 February 2010
Accepted 19 March 2010
Available online 27 March 2010

Keywords:
Ultra-high-performance liquid chromatography
Doxorubicin
Doxorubicinol

ABSTRACT

Doxorubicin, a highly effective anticancer drug, produces severe side effect such as cardiotoxicity, which is mainly caused by its metabolite, doxorubicinol. While *in vitro* studies by measuring cellular concentration of doxorubicin have been reported, there have been no reports on measuring cellular concentration of the metabolites. In this report, we developed a sensitive and high-throughput method for measuring cellular concentrations of doxorubicin and its metabolites by ultra-high-performance liquid chromatography. The method achieved more than 96% recovery of doxorubicin and its metabolites from cell homogenates. Using simple separation conditions, doxorubicin and its three main metabolites, and the internal standard, were separated within 3 min. The method has a limit of quantification of 17.4 pg (32.0 fmol) injected doxorubicin. This high sensitivity enables the detection and intracellular quantification of doxorubicin and its metabolite, doxorubicinol, in cell homogenates, and its use will facilitate studies of the relationship between doxorubicin pharmacokinetics and therapeutic outcome.

1. Introduction

The anthracycline doxorubicin, which was originally produced by *Streptomyces peucetius* var. *caesius*, is one of the most widely used anticancer agents, and it has a broad spectrum of activity against a variety of malignancies [1,2]. However, the clinical use of doxorubicin is limited by the side effect of cumulative dose-dependent irreversible chronic cardiomyopathy by doxorubicin and its metabolite, and optimal dose schedules remain a matter of debate [3]. *In vitro* studies have demonstrated a relationship between intracellular doxorubicin levels and cytotoxicity [4,5]. It was proposed that monitoring of intracellular doxorubicin concentrations could help elucidate the relationship between anthracycline pharmacokinetics and therapeutic outcome [6]. Although doxorubicinol, which is one of the major metabolites, has more potent cardiotoxic action than doxorubicin [3], there have been no reports on measuring intracellular level of doxorubicinol, probably due to the detection sensitivity. In this report, we developed a method for measuring intracellular concentrations of doxorubicin and its metabolites.

A number of methods for the simultaneous quantification of doxorubicin and its metabolites in biological samples are based on high-performance liquid chromatography (HPLC) with fluorescence detection [7–11]. Efforts to quantify anthracycline drugs in blood and tissues have encountered methodological difficulties, possibly because of a combination of failure to achieve chromatographic resolution of the various metabolites and the high affinity of these drugs for cellular constituents [12].

Ultra-high-performance liquid chromatography (UHPLC) is a new category of separation techniques that is based upon well-established principles of liquid chromatography. The resolution, sensitivity, and speed of analysis are dramatically increased by the use of 2-μm particles in the stationary phase, high linear velocities for the mobile phase, and instrumentation that operates at higher pressures than those used in HPLC [13–15].

Because doxorubicin intercalates into DNA, to achieve good recovery we used two enzymes during sample preparation that are commonly employed in the purification and degradation of DNA. By using UHPLC, we developed a simple and high-throughput method with high sensitivity for the analysis of intracellular doxorubicin and its metabolites.

2. Materials and methods

2.1. Drugs and chemicals

Doxorubicin hydrochloride and daunorubicin hydrochloride were purchased from Wako Pure Chemical Industries, Ltd. (Osaka,

Abbreviations: UHPLC, ultra-high-performance liquid chromatography; PMSF, phenylmethylsulfonyl fluoride; Triton X-100, polyoxyethylene(10) octylphenyl ether; DMEM, Dulbecco's modified Eagle's medium; FBS, fetal bovine serum.

* Corresponding author. Tel.: +81 3 3700 9662; fax: +81 3 3700 9662.
E-mail address: kumikato@nihs.go.jp (K. Sakai-Kato).

1570-0232/$ – see front matter © 2010 Elsevier B.V. All rights reserved.
doi:10.1016/j.jchromb.2010.03.040

Japan). Doxorubicinol hydrochloride and doxorubicinone were purchased from Toronto Research Chemicals Inc. (North York, Canada). Doxorubicinolone was synthesized from doxorubicinol by acidic hydrolysis (0.5 N HCl) at 50 °C for 24 h. Aglycone was extracted with chloroform by a liquid–liquid extraction method [16].

DNase I, phenylmethylsulfonyl fluoride (PMSF), proteinase K, and zinc sulfate heptahydrate were obtained from Sigma–Aldrich Corporation (St. Louis, MO, USA). Polyoxyethylene(10) octylphenyl ether (Triton X-100), magnesium chloride, sodium dihydrogen phosphate dehydrate, and phosphoric acid were obtained from Wako Pure Chemical Industries, Ltd. HPLC-grade isopropanol, HPLC-grade acetonitrile, and HPLC-grade methanol were obtained from Kanto Chemical Co., Inc. (Tokyo, Japan).

2.2. Cell culture

HeLa cells (Health Science Research Resources Bank, Osaka, Japan) and HT29 cells (American Type culture Collection, VA, USA) were cultured in Dulbecco's modified Eagle's medium (DMEM; Invitrogen Corp., CA, USA) supplemented with 10% fetal bovine serum (FBS; Nichirei Biosciences Inc., Tokyo, Japan) and 100 U/mL penicillin–streptomycin mixture (Invitrogen). Cells were grown in a humidified incubator at 37 °C and 5% CO_2.

2.3. Preparation of samples for HPLC

Cells were washed with PBS, resuspended in 300 μL PBS and lysed on ice with an ultrasonic homogenizer (Astrason, Misonix Inc., IN, USA). The lysed samples were treated with enzymes according to the method of Anderson et al. [4]. Five microliters Triton X-100 (5%) and 5 μL proteinase K (10 mg/mL) were added to an aliquot of 200 μL cell homogenates. After brief mixing, the samples were incubated for 1 h at 65 °C in a water bath. An aliquot of 2.5 μL PMSF (10 mM in isopropanol) was added and the samples were incubated for 10 min at room temperature. Then 5 μL $MgCl_2$ (0.4 M) and 10 μL DNase I (1 mg/ml) were added and the samples were incubated in a water bath at 37 °C for 30 min.

Each 225 μL sample was then mixed with 225 μL methanol and 22.5 μL $ZnSO_4$ (400 mg/mL) and centrifuged at 15,000 × *g* for 5 min in a microcentrifuge (Model 3740, Kubota Corp., Tokyo, Japan); the supernatants were then collected. A 30-μL aliquot of each supernatant was mixed with 5 μL of the internal standard (daunorubicin, 10 μg/mL in methanol), 50 μL ice-cold methanol and 15 μL Milli-Q water, and filtered through a 0.20-μm filter (Millex-LG, Millipore Corp., Tokyo, Japan). The filtrates were transferred to autosampler vials before UHPLC analysis.

The amounts of protein in cell homogenates were determined using BIO-RAD protein assay reagent (BIO-RAD, CA, USA).

2.4. HPLC apparatus

High-throughput quantification of doxorubicin and its metabolites was performed using a Hitachi LaChrom ULTRA system, equipped with an L-2160U pump, an L-2200U automated sample injector, an L-2300 thermostatted column compartment, and an L-2485U fluorescence detector (Hitachi, Tokyo, Japan).

2.5. Chromatographic conditions

Samples were analyzed on a Capcell Pak C18 IF column (2.0 × 50 mm; particle size, 2 μm; Shiseido Corp., Tokyo, Japan). The mobile phase consisted of a 50-mM sodium phosphate buffer (pH 2.0): acetonitrile mixture (65:27 v/v). The mobile phase was delivered at a rate of 300 μL/min and the column temperature was maintained at 25 °C. The fluorescence detector was operated at an excitation wavelength of 470 nm and an emission wavelength of 590 nm. A volume of 5 μL of sample was injected each time.

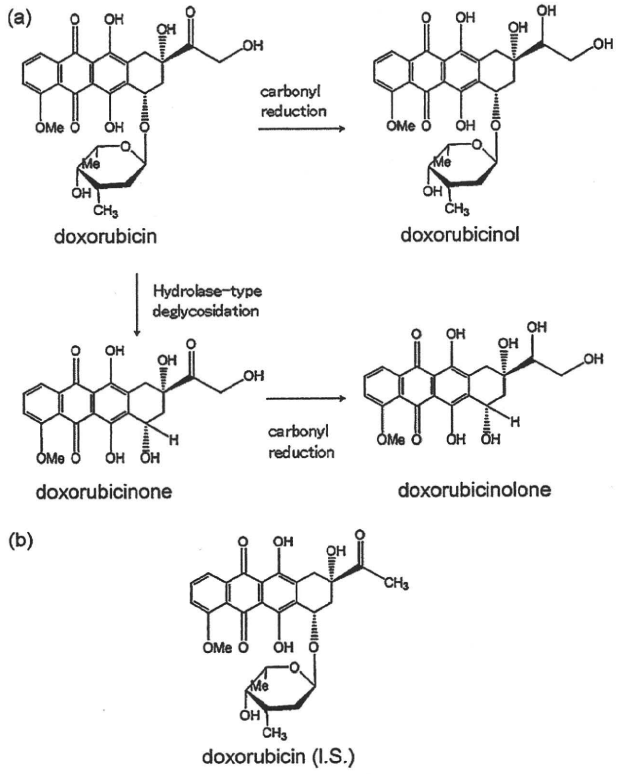

Fig. 1. Schematic showing the chemical structure of doxorubicin and its metabolites (a) and the chemical structure of daunorbicin, the internal standard (b).

2.6. Confocal analysis of live cells

The intracellular distribution of doxorubicin was examined by live-cell confocal microscopy (Carl Zeiss LSM 510, Germany). Dedicated software supplied by the microscope manufacturers was used to collect data, and images were exported as TIFF files. HeLa cells (1.5×10^5) were plated into 35-mm glass-bottomed dishes coated with poly-L-lysine (Matsunami, Osaka, Japan) and cultured in DMEM containing 10% FBS and 100 U/mL penicillin–streptomycin mix. After 2 days of incubation (37 °C, 5% CO_2), the culture medium was replaced and the cells were exposed to 1 μg/mL doxorubicin. After 1 h, cells were washed and kept in Hanks's Balanced Salt Solution (Invitrogen) for subsequent imaging by confocal microscopy.

3. Results and discussion

3.1. Chromatograms

Fig. 1a shows the chemical structure of doxorubicin and the doxorubicin metabolites that were studied in this report, and the structure of the internal standard (daunorubicin) (Fig. 1b). Because these chemicals show native fluorescence, they can be sensitively analyzed by the detection of this fluorescence. Fig. 2 shows the chromatograms resulting from the analysis of a standard solution of doxorubicin, doxorubicinol, doxorubicinolone, doxorubicinone, and the internal standard. All compounds were separated within 3 min with good resolution owing to the use of UHPLC. The pressure was 26.6 MPa at a flow rate of 300 μL/min, but the pressure was not high enough to adversely affect the stability of the column. High repeatability of analyte retention times was achieved; the relative

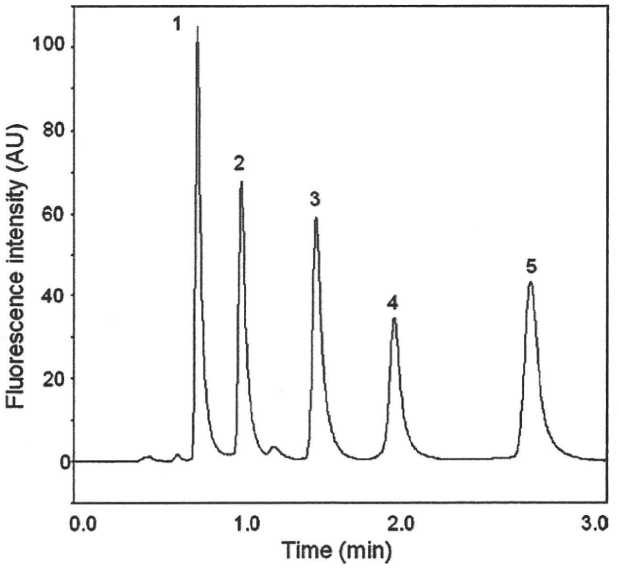

Fig. 2. Chromatogram of doxorubicin and its metabolites. The chromatographic conditions are described in Section 2. 1, doxorubicinol; 2, doxorubicin; 3, doxorubicinolone; 4, daunorubicin (internal standard); 5, doxorubicinone.

standard deviation (R.S.D.) of each peak was less than 0.13% ($n = 5$), for each analyte, at a concentration of 50 ng/mL. The conditions of separation of doxorubicin and its three metabolites were very simple in that the elution was isocratic, and the mobile phase consisted of only two different solvents, whereas some reported methods require three different solvents [7,8]. Fig. 3a is a chromatogram of a homogenate from untreated HeLa cells, and Fig. 3b is a chromatogram of an equivalent homogenate spiked with doxorubicin and its metabolites at a concentration of 500 ng/mL. No interfering peaks were observed, and doxorubicin, the three metabolites, and the internal standard separated well. These results show that the separation conditions were optimized with selectivity to each compound.

3.2. Detection limits and quantitation limits

Detection limits and quantitation limits of doxorubicin and its metabolites were determined based on the signal-to-noise approach, (S:N ratio, 3:1 for detection limits and 10:1 for quantitation limit) (Table 1). The quantitation limits of doxorubicin, doxorubicinol, doxorubicinolone, and doxorubicinone ranged between 11.7 and 24.5 pg/injection. The quantitation limit of 17.4 pg/injected doxorubicin (32.0 fmol/injected doxorubicin) was about 2 times lower than the limit ever reported using conventional HPLC [8], and more than 10 times lower than other reported values [7,9–11]. We suggest that the high resolution and sensitivity of UHPLC are responsible for this improvement.

Table 1
Detection limits and quantitation limits of doxorubicin and its metabolites.

Compound	Detection limit (pg/injection)	Quantitation limit (pg/injection)
Doxorubicin	5.2	17.4
Doxorubicinol	3.5	11.7
Doxorubicinolone	6.0	19.8
Doxorubicinon	7.4	24.5

The detection and quantitation limits of doxorubicin and its metabolites were determined based on signal-to-noise ratios (3:1 for detection limits, and 10:1 for quantitation limits).

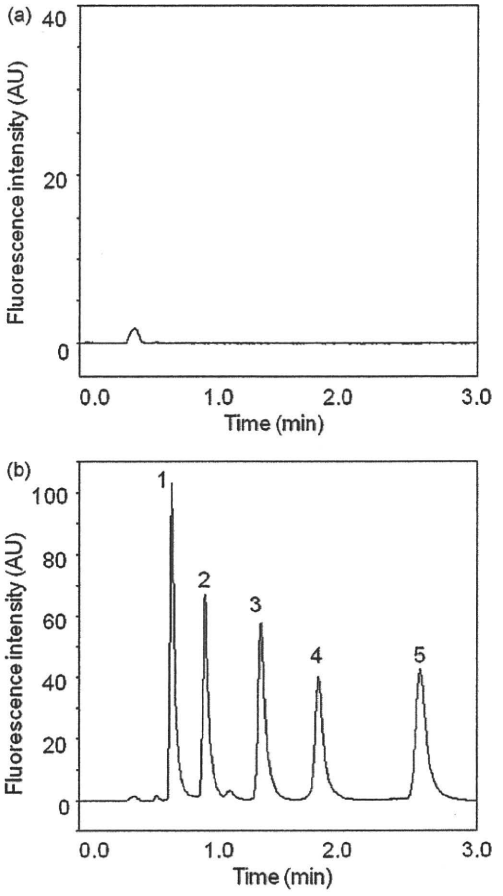

Fig. 3. Chromatograms of (a) HeLa cell homogenate and (b) HeLa cell homogenate spiked with doxorubicin and its metabolites. The chromatographic conditions were the same as in Fig. 2 and are described in Section 2. 1, doxorubicinol; 2, doxorubicin; 3, doxorubicinolone; 4, daunorubicin (internal standard); 5, doxorubicinone.

3.3. Drug recovery

Doxorubicin and its metabolites have a high affinity for cellular constituents [12]. Confocal fluorescence imaging of a HeLa cell that was exposed to doxorubicin for 1 h showed that doxorubicin had preferential affinity for the nucleus (Fig. 4). Drug recovery was assessed by adding doxorubicin, doxorubicinol, doxorubicinolone,

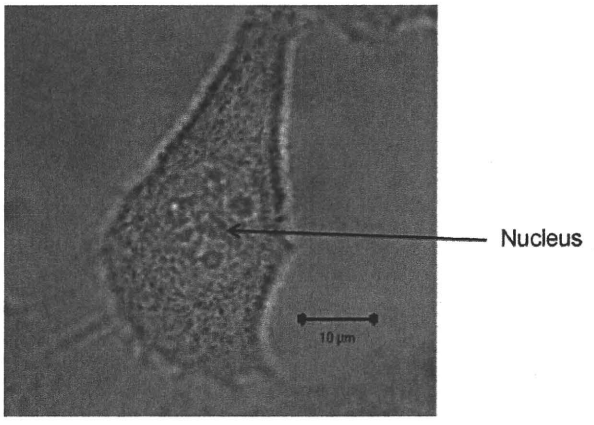

Fig. 4. Intracellular distribution of doxorubicin. HeLa cells were exposed to 1 μg/mL doxorubicin for 1 h, washed, and observed by confocal microscopy. Scale bar: 10 μm.

Table 2
The recovery of doxorubicin and its metabolites from HeLa cell homogenates.

Compound	Recovery rate	
	(%)	R.S.D. (%)
Doxorubicin	102	3.3
Doxorubicinol	105	2.9
Doxorubicinolone	96	1.4
Doxorubicinone	98	2.1

Each compound (1 μg/mL) was added to HeLa cell homogenates, which were then treated as described in Section 2. Mean values for percentage recovery are given ($n=3$).

and doxorubicinone to homogenates of two representative human cancer cell-lines, HeLa cells (derived from human epithelial carcinoma) and HT29 cells (derived from human colon adenocarcinoma grade II) before sample preparation. When the cell homogenate was treated with only methanol and $ZnSO_4$, by a method previously used to study doxorubicin and its metabolites in plasma [9], the percentage recoveries of doxorubicin, doxorubicinol, doxorubicinolone, and doxorubicinone were 84.1 ± 8.2%, 63.2 ± 3.0%, 78.4 ± 3.7%, and 88.7 ± 2.7%, respectively, ($n=3$). Doxorubicinol is harder to recover because it has higher affinity to the cellular constituents, and this affinity to the cellular constituents causes its cytotoxicity [3]. To obtain a higher drug recovery, the cells were lysed by an ultrasonic homogenizer, and the cellular proteins were further digested and solubilized with a combination of Triton X-100 and the endopeptidase proteinase K. Nuclear DNA was hydrolyzed by treatment with DNase I in the presence of divalent cations. Using these enzymatic treatments in accordance with the method of Anderson et al. [4], the recovery dramatically improved (Table 2). Furthermore, for each compound, a satisfactory within-day repeatability was achieved with R. S. D. of ≤ 3.3%, $n=3$.

3.4. Linearity of the calibration plots

We created calibration plots for doxorubicin, doxorubicinol, doxorubicinolone, and doxorubicinone (Fig. 5). The *y*-axis is the ratio of the peak area of each analyte tested to the peak area of the internal standard (daunorubicin), and the *x*-axis is the concentra-

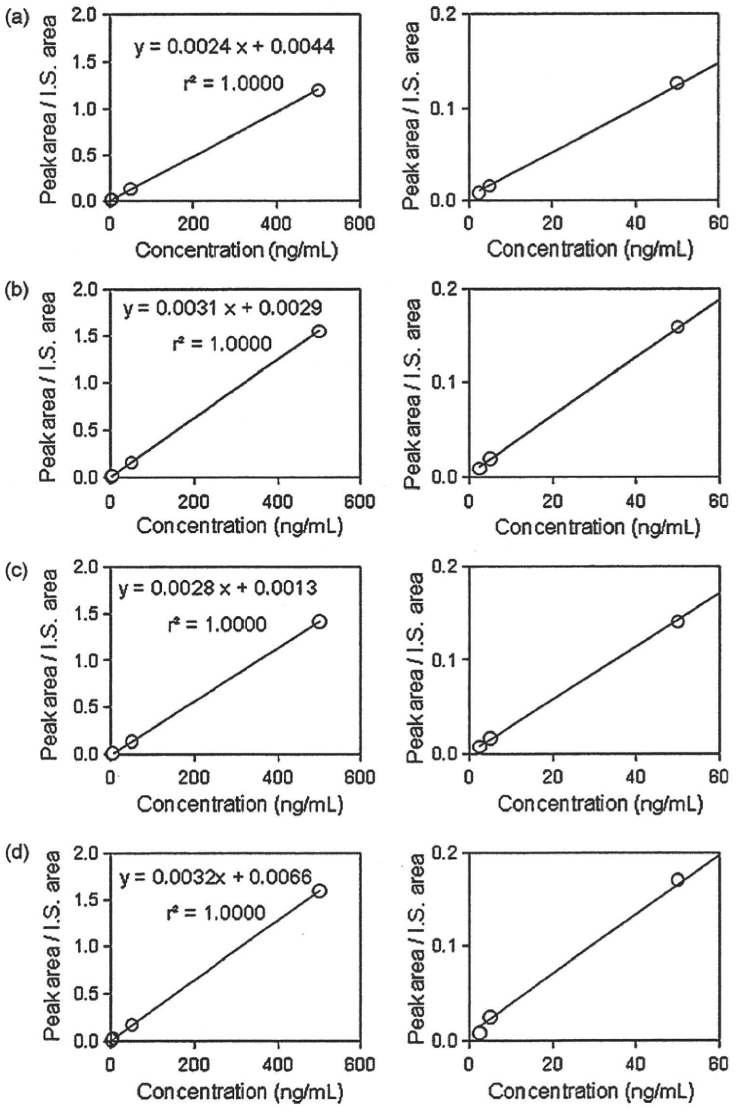

Fig. 5. Linearity of the calibration curves of doxorubicin and its metabolites. Calibration plots for (a) doxorubicin, (b) doxorubicinol, (c) doxorubicinolone, and (d) doxorubicinone. The left and right panels show results for the same HPLC run, but the plots in the right panel focus on the lower concentration ranges. I.S. denotes internal standard.

Table 3
Quantitation of doxorubicin and doxorubicinol in homogenates prepared from doxorubicin-treated cells.

Sample	Doxorubicin (μg/mg cell protein)	Doxorubicinol (μg/mg cell protein)
HeLa cells	3.4 ± 0.55	0.057 ± 0.0060
HT29 cells	3.5 ± 0.38	0.048 ± 0.0029

Cells were treated for 2 h with 10 μg/mL doxorubicin, and cell homogenates were prepared and analyzed, as described in Section 2. Values are given as mean ± S.D. (n (dish number) = 3).

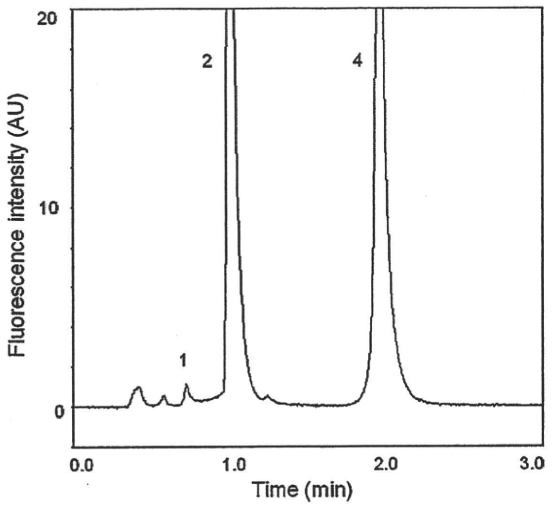

Fig. 6. Chromatogram of cell homogenate obtained 2 h after administration of doxorubicin. HeLa cells were exposed to 10 μg/mL doxorubicin for 2 h. Cell homogenates were then prepared as described in Section 2. 1, doxorubicinol; 2, doxorubicin; 3, daunorubicin (internal standard).

tion of the corresponding analyte. The plots were linear over a wide range of concentrations (r^2 = 1.0; Fig. 5).

3.5. Quantitative determination of the levels of doxorubicin and its metabolite in cells

The validated method described above was used for the simultaneous determination of doxorubicin and its metabolites in human cancer cell-lines. HeLa cells and HT29 cells were exposed to 10 μg/mL doxorubicin for 2 h, and then washed with PBS. Chromatograms of the cell homogenates were obtained by UHPLC (Fig. 6). As shown, doxorubicin and one of its metabolites, doxorubicinol, were detected in cell homogenates (Fig. 6). The results of quantitative determination of doxorubicin and doxorubicinol are shown in Table 3. Values are expressed as amounts per 1 mg cellular protein in each dish, due to the diversity of cell numbers for different dishes, and values are given as mean ± S.D. for three dishes of the same cell type. The S.D. values for different dishes of the same cell type were acceptable. Doxorubicinol is produced by cytosolic carbonyl reductase through the NADPH-dependent aldo-keto reduction of a carbonyl moiety in doxorubicin [17]; our results first demonstrated that both human cancer cell-lines, HeLa cells and HT29 cells, produced doxorubicinol from doxorubicin. In contrast, our results showed that deglycosidation at the daunosamine sugar in doxorubicin, which produces doxorubicinone and doxorubicinolone (Fig. 1a) [17], was negligible in these cancer cell-lines (Fig. 6).

New formulation technologies that aim to enhance the effectiveness and safety of anticancer drugs are currently being developed. For instance, long-circulating and sterically stabilized liposomes containing doxorubicin can markedly increase tumor-specific deposition of drugs and have been approved as clinical products [18]. Other carrier systems such as polymer micelles [19,20] are also being developed for use with doxorubicin. In these technologies, effective release of doxorubicin from the carrier into the target cells is important for effectiveness and safety. Direct quantification of the metabolites may facilitate the assessment and comparison of doxorubicin release from carriers, since it is presumed that metabolism of doxorubicin takes place only after its release from the carriers. Analytical methodology that enables the rapid quantification of doxorubicin and its metabolites, particularly in targeted tumor cells, will facilitate the optimization of carrier-based strategies for doxorubicin delivery and will help provide insight into the toxicity and bioavailability of doxorubicin incorporated into carriers such as liposomes or polymer micelles.

4. Conclusions

Our results show that this methodology provides a significant reduction in analysis time and a considerable increase in assay sensitivity. We demonstrated that the method is sensitive enough to quantify the levels of doxorubicin and its metabolite within cells, and we predict that it will greatly facilitate studies of doxorubicin pharmacokinetics and clarify the effect of doxorubicin metabolism on therapeutic outcome at the cellular level. Furthermore, this method can be applied to the evaluation of emerging formulation technologies that are based on encapsulated doxorubicin.

Acknowledgements

The authors are grateful for financial support from the Research on Publicly Essential Drugs and Medical Devices Project (The Japan Health Sciences Foundation), a Health Labor Sciences Research Grant from the Ministry of Health, Labour and Welfare (MHLW), and KAKENHI (21790046) from the Ministry of Education, Culture, Sports, Science, and Technology (MEXT), Japan.

References

[1] G.N. Hortobagyi, Drugs 54 (1997) 1.
[2] A. Di Marco, M. Gaetani, B. Scarpinato, Cancer Chemother. Rep. 53 (1969) 33.
[3] R.D. Olson, P.S. Mushlin, D.E. Brenner, S. Fleischer, B.J. Cusack, B.K. Chang, R.J. Boucek Jr., Proc. Natl. Acad. Sci. U.S.A. 85 (1988) 3585.
[4] A. Anderson, D.J. Warren, L. Slordal, Cancer Chemother. Pharmacol. 34 (1994) 197.
[5] S. Licata, A. Saponiero, A. Mordente, G. Minotti, Chem. Res. Toxicol. 13 (2000) 414.
[6] B. Sundman-Engberg, U. Tidefelt, J. Liliemark, C. Paul, Cancer Chemother. Pharmacol. 25 (1990) 252.
[7] Q. Zhou, B. Chowbay, J. Pharm. Biomed. Anal. 30 (2002) 1063.
[8] J.V. Aspere, O.V. Tellingen, J.H. Beijnen, J. Chromatogr. B: Biomed. Sci. Appl. 712 (1998) 129.
[9] A. Andersen, D.J. Warren, L. Slordal, Ther. Drug Monit. 15 (1993) 455.
[10] S. Shinozawa, Y. Mimaki, Y. Araki, T. Oda, J. Chromatogr. 196 (1980) 463.
[11] L.M. Rose, K.F. Tillery, S.M. el Dareer, D.L. Hill, J. Chromatogr. 425 (1988) 419.
[12] A. Andersen, H. Holte, L. Slordal, Cancer Chemother. Pharmacol. 44 (1999) 422.
[13] M.E. Swartz, J. Liq. Chromatogr. Relat. Technol. 28 (2005) 1253.
[14] L. Novakova, H. Vlckova, Anal. Chim. Acta 656 (2009) 8.
[15] N. Sun, G. Lu, M. Lin, G. Fan, Y. Wu, Talanta 78 (2009) 506.
[16] K.E. Maudens, C.P. Stove, W.E. Lambert, J. Sep. Sci. 31 (2008) 1042.
[17] S. Takanashi, N.R. Bachur, Drug Metab. Dispos. 4 (1976) 79.
[18] M.E.R. O'Brien, N. Wigler, M. Inbar, R. Rosso, E. Grischke, A. Santoro, R. Catane, D.G. Kieback, P. Tomczak, S.P. Ackland, F. Orlandi, L. Mellars, C. Tendler, Ann. Oncol. 15 (2004) 440.
[19] M. Yokoyama, T. Okano, Y. Sakurai, S. Fukushima, K. Okamoto, K. Kataoka, J. Drug Target. 7 (1999) 171.
[20] T. Nakanishi, S. Fukushima, K. Okamoto, M. Suzuki, Y. Matsumura, M. Yokoyama, T. Okano, Y. Sakurai, K. Kataoka, J. Control. Release 74 (2001) 295.

International Journal of Pharmaceutics 407 (2011) 111–118

Contents lists available at ScienceDirect

International Journal of Pharmaceutics

journal homepage: www.elsevier.com/locate/ijpharm

Differences in crystallization rate of nitrendipine enantiomers in amorphous solid dispersions with HPMC and HPMCP

Tamaki Miyazaki[a,*], Yukio Aso[a], Sumie Yoshioka[b], Toru Kawanishi[a]

[a] Division of Drugs, National Institute of Health Sciences, 1-18-1 Kamiyoga, Setagaya-ku, Tokyo 158-8501, Japan
[b] School of Pharmacy, University of Connecticut, Storrs, CT, United States

ARTICLE INFO

Article history:
Received 21 October 2010
Received in revised form
21 December 2010
Accepted 19 January 2011
Available online 26 January 2011

Keywords:
Nitrendipine
Enantiomer
Chiral polymer
Solid dispersions
Crystallization

ABSTRACT

To clarify the contribution of drug–polymer interaction to the physical stability of amorphous solid dispersions, we studied the crystallization rates of nitrendipine (NTR) enantiomers with identical physicochemical properties in the presence of hydroxypropylmethylcellulose (HPMC), hydroxypropylmethylcellulose phthalate (HPMCP) and polyvinylpyrrolidone (PVP). The overall crystallization rate at 60 °C and the nucleation rate at 50–70 °C of (+)-NTR were lower than those of (−)-NTR in the presence of 10–20% HPMC or HPMCP. In contrast, similar crystallization profiles were observed for the NTR enantiomers in solid dispersions containing PVP. The similar glass transition temperatures for solid dispersions of (−)-NTR and (+)-NTR suggested that the molecular mobility of the amorphous matrix did not differ between the enantiomers. These results indicate that the interaction between the NTR enantiomers and HPMC or HPMCP is stereoselective, and that differences in the stereoselective interaction create differences in physical stability between (−)-NTR and (+)-NTR at 50–70 °C. However, no difference in physical stability between the enantiomers was obvious at 40 °C. Loss of the difference in physical stability between the NTR enantiomers suggests that the stereoselective interaction between NTR and the polymers may not contribute significantly to the physical stabilization of amorphous NTR at 40 °C.

1. Introduction

Nifedipine analogues are used for treatment of cardiovascular disorders. Most of them are poorly water soluble and their bioavailability is low when administered orally in crystal form. To improve the bioavailability by increasing the dissolution rate and solubility, amorphous solid dispersions of nifedipine analogues have been studied over the past few decades (Suzuki and Sunada, 1998; Chutimaworapan et al., 2000; Vippagunta et al., 2002; Hirasawa et al., 2003a,b, 2004; Tanno et al., 2004; Karavas et al., 2005, 2006; Wang et al., 2005, 2007; Kim et al., 2006; Konno and Taylor, 2006; Huang et al., 2008; Marsac et al., 2008; Rumondor et al., 2009a,b). Drugs in an amorphous state are more easily dissolved in water than their crystalline counterparts. However, recrystallization to a thermodynamically stable form during long-term storage is a matter of concern. The physical stability of amorphous solid dispersions (crystallization tendency) has been reported to correlate with several factors, such as molecular mobility (Aso et al., 2004; Miyazaki et al., 2007), drug–excipient interactions and miscibility (Matsumoto and Zografi, 1999; Marsac et al., 2006, 2009; Miyazaki et al., 2004, 2006, 2007; Konno and Taylor, 2006; Haddadin et al., 2009; Tao et al., 2009; Telang et al., 2009). The crystallization rate of amorphous nitrendipine (NTR) increases with a decrease in the glass transition temperature (T_g) associated with water sorption, indicating that molecular mobility, in terms of T_g, is correlated with physical stability. However, amorphous nilvadipine is more stable than nifedipine, even though the two had similar T_g values, indicating that the difference in physical stability between nilvadipine and nifedipine might be attributable to differences in chemical structure (Miyazaki et al., 2007). Hydrogen bond interaction between felodipine and hydroxypropylmethylcellulose (HPMC) or hydroxypropylmethylcellulose acetate succinate is considered to decrease the nucleation rate of felodipine, since no significant change in molecular mobility, reflected in T_g value, has been observed (Konno and Taylor, 2006). Also, drug–excipient miscibility is reportedly related to the physical stability of nifedipines. Drug crystallization has been observed to occur earlier in solid dispersions showing phase separation due to low miscibility of the drug with the excipient polymers (Rumondor et al., 2009a,b; Marsac et al., 2010). In order to develop stable amorphous solid dispersions, it is important to clarify the relative significance of these factors for the physical stability of amorphous solid dispersions. Therefore, designing a model system that is as simple as possible is the key to evaluation of each individual factor.

NTR has an asymmetric carbon (Fig. 1), and is available as a mixture of both enantiomers. These enantiomers can be resolved by chiral chromatography. Since both enantiomers have identical physical and chemical properties, including molecular mass, T_g,

* Corresponding author. Tel.: +81 3 3700 1141; fax: +81 3 3707 6950.
E-mail address: miyazaki@nihs.go.jp (T. Miyazaki).

0378-5173/$ – see front matter © 2011 Elsevier B.V. All rights reserved.
doi:10.1016/j.ijpharm.2011.01.035

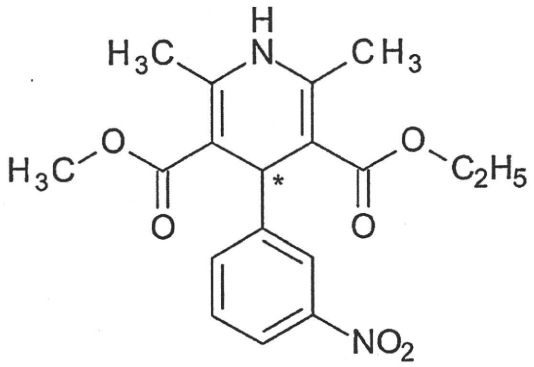

Fig. 1. Chemical structure of NTR. The asterisk represents asymmetric carbon.

melting point and density, the effects of molecular mobility and chemical structure on their physical stability are expected to be the same. Therefore, solid dispersions of NTR enantiomers may provide a useful model system for studies of drug–polymer stereoselective interaction. In the present study, HPMC and hydroxypropylmethylcellulose phthalate (HPMCP) were used as chiral polymers, and polyvinylpyrrolidone (PVP), an achiral polymer, was selected as a control to investigate the effect of drug–polymer interaction on the physical stability of amorphous NTR enantiomers. The overall crystallization rates were determined from the time-profiles of amorphous drug remaining, as measured by differential scanning calorimetry (DSC). Furthermore, the nucleation and the crystal growth rates of each NTR enantiomer in the solid dispersions containing HPMC, HPMCP or PVP were determined by polarized light microscopy. Measurements of T_g and Fourier-transform infrared spectra (FT-IR) were carried out for evaluation of molecular mobility and drug–polymer interactions, respectively.

2. Materials and methods

2.1. Materials

PVP (PVP10) and HPMC (USP grade) were purchased from Sigma–Aldrich, Inc. HPMCP (HP-55) was kindly obtained from Shin-Etsu Chemical Co., Ltd.

NTR (Wako Pure Chemical Industries Ltd.) was resolved on a CHIRALCEL OJ-H column (Daicel Chemical Industries, Ltd., 10 mm × 250 mm) into two fractions of each enantiomer with a mobile phase of n-hexane/ethanol (100/15, flow rate: 4 ml/min). A 500 μl of 1% NTR solution in n-hexane/ethanol (1/1) was injected, and ultraviolet spectrophotometric detection was carried out at 254 nm. The circular dichroism spectrum of the first fraction exhibited a negative peak at around 360 nm, and the second one exhibited a positive peak. Therefore, the first and second fractions of NTR were designated (−)-NTR and (+)-NTR, respectively. The optical purity of each enantiomer was determined to be more than 99.96%, and the amount of photo degradation product of NTR was determined to be less than 0.03% by liquid chromatography, on a CHIRALCEL OJ-H column (Daicel Chemical Industries, Ltd.,

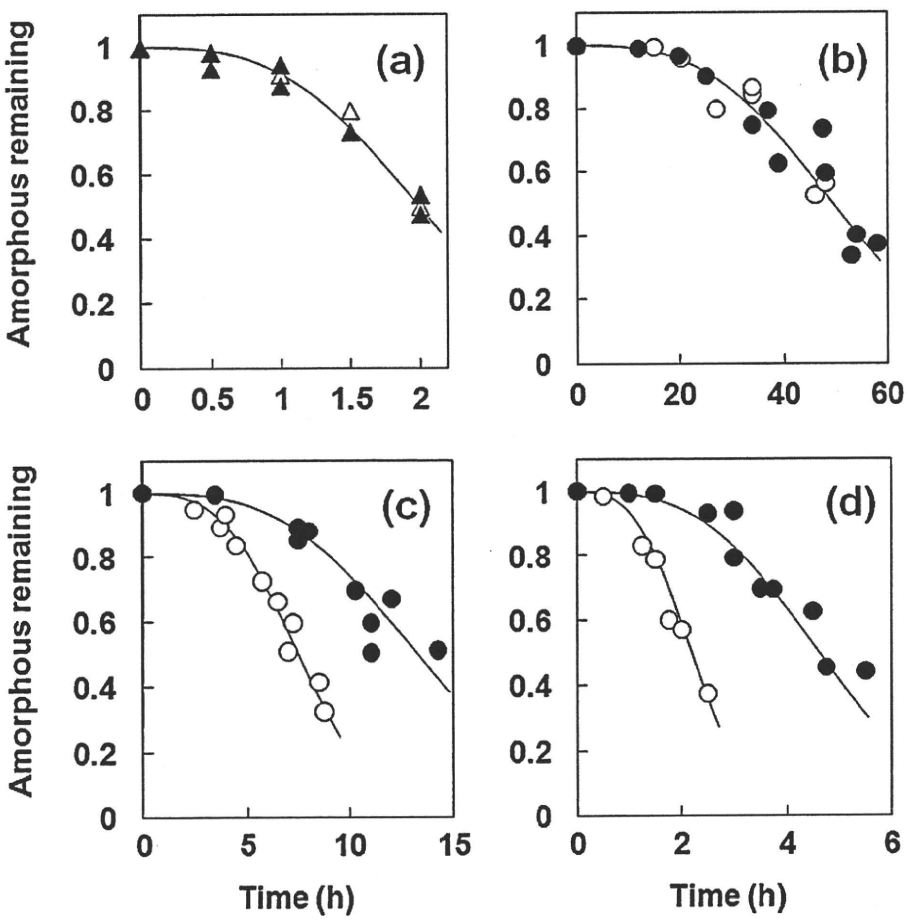

Fig. 2. Crystallization profiles of each NTR enantiomer alone ((a); △, ▲) and the enantiomers in solid dispersions (○, ●) with (b) 10% PVP, (c) 10% HPMC and (d) 10% HPMCP at 60 °C. Open symbols represent (−)-NTR and solid symbols represent (+)-NTR. The lines in the figures represent the best fit of the Avrami equation.